THE HOLOGRAPHIC STEREOGRAM

Thesis by

John T. McCrickerd

In Partial Fulfillment of the Requirements

For the Degree of

Doctor of Philosophy

California Institute of Technology

Pasadena, California

1969

(Submitted May 20, 1969)

ACKNOWLEDGMENTS

I wish to thank Professor Nicholas George for the consistently first-rate scientific guidance he has provided through the course of this research, and for his fine friendship. His sincerely positive and enthusiastic attitude toward new ideas and his unfailing sense of humor have certainly helped to make my years at Caltech worthwhile and enjoyable.

I thank Milton M. T. Chang and Dr. John W. Matthews for many enlightening discussions. For ceaselessly and voluntarily contributing invaluable references, I thank Paula Samazan. Held in highest esteem for their ability to transform the merest of sketches into working machinery are Norm Keidel and Don Laird. I wish it were possible for me to sufficiently express my gratitude to all the others who have also so enthusiastically cooperated in this work. A special note of thanks, though, is due Mrs. Joan Schuetz for her masterful typing of the manuscript.

I am particularly grateful to my wife, Eileen, for her work and patience which helped make this thesis possible.

Finally, I appreciate the support of the Electronics Division of the U. S. Air Force Office of Scientific Research, and of the Traineeship program of the National Science Foundation.

ABSTRACT

The holographic stereogram, a hologram synthesized from ordinary stereoscopic component photographs, is investigated as an alternative to classical holograms and to previous types of stereograms for three-dimensional perfect imagery. The process is partly holographic in nature, but it provides images of naturally illuminated objects, and its application is not limited by the technology of laser illumination. The pinhole camera stereogram and the fly's eye lens stereogram are also analyzed, since the principles of their operation are similar. Pinhole camera stereogram imagery is shown to have several deficiencies, among which is the necessity for small camera-object distances. The fly's eye lens is much superior, but is limited in practice by aberrations, a difficulty which the holographic stereogram overcomes. Also treated are the full-color, the focused-type, and the distortionless-scaled holographic stereogram, and optical spatial filtering of holographic stereogram images.

The achromatically imaged Fresnel zone plate is analyzed as a technique of very general applicability which compensates for source incoherency in two-beam type holographic arrangements. The emphasis is on physical interpretation rather than mathematical formulation. Two simple graphical mnemonics are developed for rapid analytical inspection of the effects of, respectively, temporal and spatial incoherence of the source in any achromatically imaged zone plate or Gabor in-line type holographic system.

The scalar wave function approximation of physical optics is used throughout.

TABLE OF CONTENTS

CHAPTER	SECTION	TITLE	PAGE
I		INTRODUCTION	1
	1.1	Introduction to Holography	1
	1.2	Introduction to Three-Dimensional Perfect Imagery	2
	1.3	Summary of Text	6
II		THE PINHOLE CAMERA STEREOGRAM	8
	2.1	Introduction	8
	2.2	The Pinhole Camera and Diffraction Focusing	10
	2.3	Three-Dimensional Imagery with the Pinhole Camera Stereogram	16
III		THE FLY'S EYE LENS STEREOGRAM	23
	3.1	Introduction	23
	3.2	The Focus Cue and General Photographic Applications	24
	3.3	Choosing Parameters for the Fly's Eye Lens	27
	3.4	Aberrations of the Fly's Eye Lenslet	31
	3.5	Comparison of Stereogram Imagery with Ordinary Photography	40
IV		THE HOLOGRAPHIC STEREOGRAM	42
	4.1	Introduction	42
	4.2	Description of the Holographic Stereogram Process	43
	4.3	The Wild Eyepiece as a Holographic Stereogram Camera	48

CHAPTER	SECTION	TITLE	PAGE
	4.4	Choosing Parameters for the Holographic Stereogram Camera	54
	4.5	Exact Form of the Holographic Stereogram Image	58
V		THE ACHROMATICALLY IMAGED FRESNEL ZONE PLATE	68
	5.1	Introduction	68
	5.2	Application to the Holographic Stereogram System	70
	5.3	Equivalence, with respect to Source Coherency Requirements, of the Imaged Zone Plate to Gabor In-Line Holography	73
		5.3.1 Temporal Incoherence	73
		5.3.2 Combined Spatial and Temporal Incoherence, and the Modulated Zone Plate Image Concept	74
	5.4	Source Coherency Requirements for Imaged Zone Plate and Gabor In-Line Holograms	76
		5.4.1 Temporal Incoherence Effects	76
		5.4.1.1 A Method for Quick Inspection	76
		5.4.2 The Effects of Finite Source Size	78
		5.4.2.1 A Simple Mnemonic	79
	5.5	An Example	81
VI		OTHER FEATURES OF THE HOLOGRAPHIC STEREOGRAM	83
	6.1	Introduction	83
	6.2	Practical Advantages of the Process	84
	6.3	The Full-Color Stereogram	85

CHAPTER	SECTION	TITLE	PAGE
	6.4	Distortionless Scaling	86
	6.5	The Focused-Type Holographic Stereogram	86
	6.6	Spatial Filtering of Holographic Stereogram Images	88
VII		CONCLUSIONS	91
APPENDIX I – ABERRATIONS OF THE FLY'S EYE LENSLET			97
APPENDIX II – HOLOGRAPHIC STEREOGRAM FROM SEQUENTIAL COMPONENT PHOTOGRAPHS			100
APPENDIX III – THE EFFECTS OF EXTREME DISTORTION – A SIMPLE EXAMPLE			103
APPENDIX IV – ACHROMATIC INCOHERENT IMAGERY OF A FRESNEL ZONE PLATE WITH ONE OF THE FIRST ORDER DIFFRACTED WAVES ELIMINATED			107
APPENDIX V – SCALING AND RESOLUTION OF SCENIC HOLOGRAPHIC STEREOGRAMS			110
REFERENCES			115

CHAPTER ONE

INTRODUCTION

1.1 Introduction to Holography

The work described here is an application of holography. There is very little consideration of the holographic process itself – extensive literature is already available on this subject.[1-5] Holography is treated here merely as a tool for the reconstruction of optical fields and images; when it is necessary to physically recall a field which had previously existed, the operation is treated quite casually. The holographic processes required here are quite simple and easy to perform. In fact, one of the main difficulties in holography – the requirement of extreme mechanical stability – is avoided; because of the small size of the component holograms of the holographic stereogram, high concentration of even weak laser beams ($\sim$ 1 mw. output) permits exposure times of less than one second.

For the benefit of the reader completely unfamiliar with holography, a very brief qualitative description of the simplest types of holograms is presented here – this should be a sufficient basis for understanding the remainder of this thesis.

Consider an object, illuminated with a coherent light beam, which is viewed through a glass plate. The plate is additionally illuminated with a plane (reference) wave derived from the same light source, and the "cross – product" term of the intensity is thus proportional to the object (reflected from the object) beam. If the resulting interference pattern is photographically deposited

and then illuminated with an identical plane wave, the object beam is reconstructed beyond the plate. If the reference beam is introduced from the same side of the plate as the object beam, we obtain a "transmission" hologram which is then viewed by looking through the plate in the direction toward the source in order to observe the perfect* and virtual "true" image. If the object and reference beams strike the plate from opposite sides, the perfect virtual true image is viewed through the plate with the source shining over the viewer's shoulder, and this is called for obvious reasons a "reflection" hologram. If either a transmission or reflection hologram is viewed from the "wrong" side, with illumination also from the "wrong" side, a pseudoscopic but perfect real image can be observed which is generally called the "conjugate", as opposed to true, image. The conjugate image phenomenon is quite easily interpreted – the wave exciting the hologram is propagating backwards (time-reversed, if you wish) and the excited conjugate image wavefronts are merely the true image waves propagating backwards to the apparent object position.

1.2 Introduction to Three-Dimensional Perfect Imagery

This thesis describes an application of holography to three dimensional imagery of incoherently illuminated scenes. The method is applicable to the imagery of large scenes, where the use of classical holographic techniques is precluded by the technical limitations of laser illumination. The "holographic stereograms" described here provide better images than those of previous types

---

* congruent with the object.

of stereograms, but which are generally not as finely resolvable as those of classical holograms of similar dimensions.

The methods here described permit an "almost-perfect" imaging of a three-dimensional object space. Every curve of the object space is geometrically similar to a curve lying within the bounds of its slightly non-stigmatic, or non-sharp, image. An everyday example of perfect imaging is that of a pair of good quality mirrors, which provide an image which is almost indistinguishable from its object; such a system is called an absolute instrument.[6] The slightly degraded image resulting from a light condensation of steam on one of the mirrors could be called almost-perfect.

Many previous methods of 3-D photography do not produce 3-D images. In the viewing of a stereo pair, for example, one's eyes focus at a fixed distance-the degree of binocular convergence exerted to eliminate parallax between the two-dimensional retinal images is mentally translated into a distance interpretation. In contrast, the viewer of a holographic stereogram must also accommodate the power of the lenses of his eyes.

The basic principles of image formation used here are easily understood in terms of geometrical optics. Stigmatic images exist where all rays intersect which emanate from a given object point. Ray intensities are proportional to object brightness, and image brightness is proportional to the intensities of the associated rays. If we specify all the rays passing through the entrance pupil, or any other pupil, of an optical system, then all the rays in the image space are determined (by any of the standard ray tracing methods). We can, therefore, by recording and later reconstructing the rays passing through a surface of an absolute instrument, so reconstruct a perfect image of the object.

It is obvious that a thin window is an absolute instrument, since the virtual image seen through the window is congruent with the object. Holographic wavefront reconstruction on a thin plate of glass,* therefore, provides us with a perfect image. A similar image results from ray reconstruction on a plate comprising the holographic stereogram, although there are several fundamental differences.

The classic hologram comprises an almost exact reconstruction of the optical wavefront emanating from a coherently illuminated scene. This wavefront is a coherent superposition of spherical waves whose sources are microscopic radiators on the surface of the object, when the object is opaque. A ray is defined as a line whose direction is everywhere normal to the associated spherical wavefront; hence the rays from each object point are a continuum of radially directed straight lines.

In the first step of synthesizing a stereogram, the superimposed spherical wavefronts from an incoherently illuminated scene are measured on small segments of a reference surface, and there is no mutual coherence between measurements on different segments. In Section 4.5 it is shown that in general the data so obtained are insufficient to permit faithful reconstruction of the spherical wavefronts, and one cannot precisely determine their centers of curvature. Stated differently, the ultimate angular resolution of the reconstructed scene, observed from the point of view of a given segment, is of the order of $\lambda/2a$, where λ is the wavelength of light and $2a$ is the segment width. The data are collected

---

*The conjugate image of a thick plate hologram is also perfect, but the true image is not, since sphericity of a wavefront is not generally preserved upon traversal of a thick piece of glass.

by means of two dimensional images and in practice a resolution somewhat worse than $\lambda/2a$ is typically attained. In contrast, the angular resolution of a classical hologram can in principle be of the order of λ/W, where W is the hologram width. We see that, although the rays of a hologram reconstruction are radially directed, some blurring inevitably occurs, and we must use physical optics to fully describe the image on a microscopic scale. We shall also have to use physical optics to understand the stereogram, but, keeping in mind the limitations on image resolution, a description in terms of ray optics is appropriate if the rays in the following discussions are interpreted as having a width of the order of $d\lambda/2a$, where d is the distance from the point of the ray's intersection with the reference surface; the use of this artifice will be justified in Sections 2.3 and 3.3.

Another distinction from ordinary geometrical optics and the hologram is that we here reconstruct a discrete number of rays from any given point on the surface of the object. The image is no less well defined for this, however, since such discreteness does not preclude intersection of the rays at the image point.

To summarize, we reconstruct a 3-D image by recording and reconstructing the rays emanating from each object point, on a reference surface comprised of a discrete number of segments. From any object point, we reconstruct one ray for each surface segment (unless the respective rays are obstructed by other portions of the object scene).

Several methods have been used to construct stereograms or integral photographs, each of which uses a different means for reconstructing, on segments of a reference surface, the rays associated with each object point. The word ray

is used in the loose sense, and it will be shown that under certain circumstances rays of width $\sim d\lambda/2a$ can be reconstructed using each of the methods. The pinhole camera array, the fly's eye lens array and its adaptation to holography due to Pole, and the holographic stereogram are described here.

1.3 Summary of Text

In Chapter Two, the concepts of geometrical cues and diffraction cues are put on firm analytical ground and applied to a study of the stereogram comprised of an array of pinhole cameras. It is shown that a rather unsatisfactory compromise between image resolution, image sharpness, and the completeness of the cone of rays contributing to a reconstructed image point must be reached, and also that the pinhole camera array must be placed close to the object.

In Chapter Three, the geometrical cue concept is extended to that of the focus cue, which is then applied to the fly's eye lens stereogram as well as to the general problem of photographic depth of focus which it resolves with an extremely simple mnemonic. While the fly's eye lens stereogram overcomes the limitations of the pinhole camera, it is found to be severely limited by aberrations in most practical cases.

In Chapter Four we describe the holographic stereogram, which overcomes the problem of aberrations. A practical stereogram camera whose main component is a wide angle eyepiece is described. The exact form of the reconstructed image is derived for the special case of a relatively flat object.

The achromatically imaged Fresnel zone plate is analyzed in Chapter Five. This is a technique of very general applicability in holography which

compensates for source incoherency. Similar techniques have previously been described in mathematical form – the present treatment is more physical in contrast. Simple graphical mnemonics are derived which facilitate rapid analytical inspection of the effects of source incoherency in any imaged zone plate or Gabor in-line type holographic system. The results are applied specifically to the holographic stereogram system.

In Chapter Six are briefly discussed some notable advantages of the holographic stereogram over the hologram or the fly's eye lens stereogram, or both. In addition to simple practical matters we treat here the color stereogram, the distortionless scaled stereogram, the focused stereogram, and spatial filtering of stereogram images.

Conclusions are presented in Chapter Seven.

CHAPTER TWO

THE PINHOLE CAMERA STEREOGRAM

2.1 Introduction

The first practical test of the principle of the stereogram, or integral photograph, was made by the pinhole camera method by P. P. Sokolov.[7] Of the many variations of the pinhole camera method, we consider one which results in the reconstruction of a pseudoscopic real image congruent with the object position. By using other variations, we could obtain images which are identical except for being orthoscopic, virtual, or reflected across the reference surface. The present case is chosen for its simplicity. Furthermore, measurements are facilitated by mechanical access to the real image – a telescope would be required for close scrutiny of a virtual image. For further simplification of the presentation, we shall treat opaque objects immersed in a homogeneous medium (air) – the extension to more general cases is obvious.

In Fig. 1 is shown a typical segment Σ of the reference surface on which rays are recorded by the pinhole camera. The segment Σ, which we consider to be very small, comprises the aperture of the camera. A ray from point 0 on the object's surface which enters the camera through Σ leaves a latent image point on the film at I. If, after reversal development, we return the film to its place and illuminate it from the side opposite Σ, some of the light from I will pass through Σ. This ray of light will obviously intersect the point 0, where the object had previously been located. We say that the

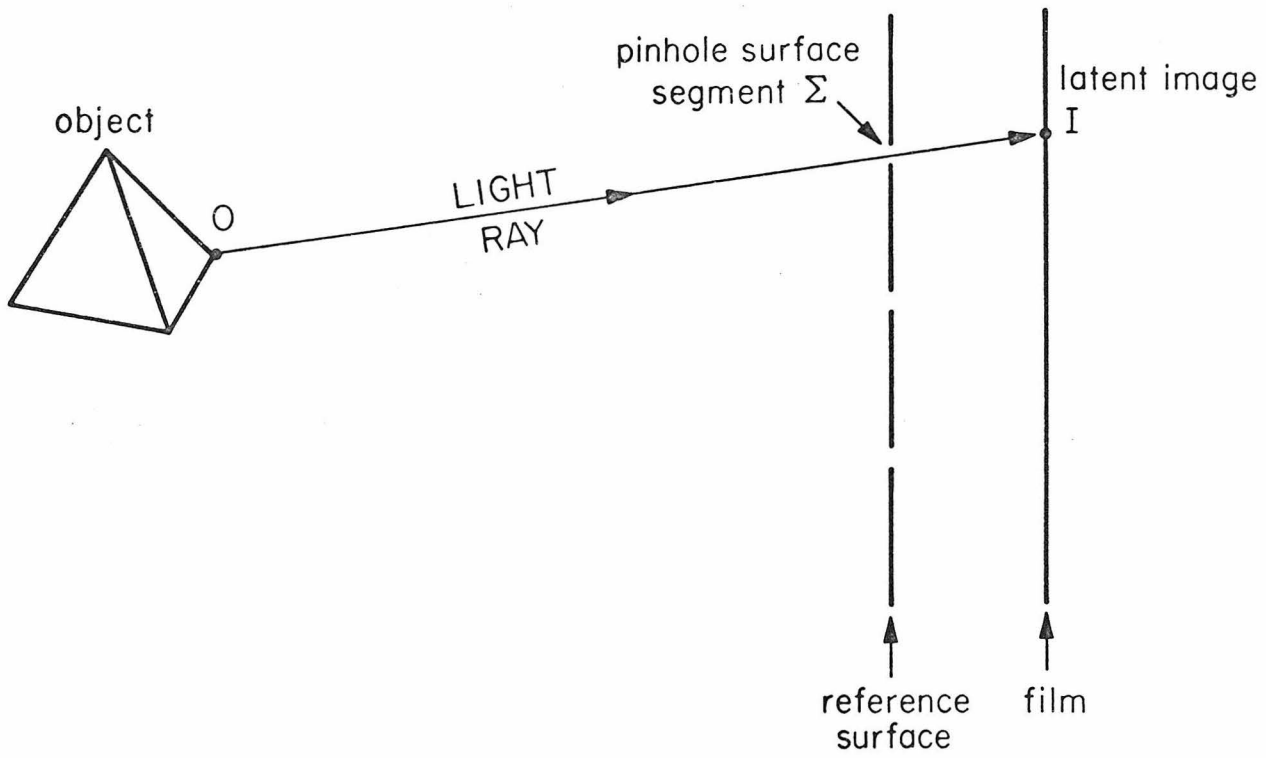

Fig. 1 Recording the pinhole camera stereogram. After reversal development of the latent image, the film is returned to its place and illuminated from the right side, for viewing of a pseudoscopic real image from the left side of position 0.

ray 0Σ has been reconstructed, although the direction of propagation has been reversed.

If n pinhole cameras are located on the reference surface, $\Sigma_1, \Sigma_2, \ldots, \Sigma_n$, there will result n rays $\Sigma_1 0, \Sigma_2 0, \ldots, \Sigma_n 0$ which intersect at the point 0.* This happens similarly for each point on the surface of the object and hence a real image is formed. The image is pseudoscopic, since the rays have been reversed in direction.

2.2 The Pinhole Camera and Diffraction Focusing

It is very convenient to understand the imaging properties of the pinhole camera, and indeed of any camera system, in terms which are as completely divorced as possible from the details of the phenomena occurring on the film plane. To this end we shall develop the concepts of the geometrical cue and diffraction cue for the pinhole camera. Scalar theory is used.

Consider a pinhole camera used to image an object contained in a plane perpendicular to the optic axis. A point object at a transverse coordinate X close to the axis produces a circularly symmetrical image which is centered at the point x on the film. We find that $x = M X$, where M is a constant, the magnification. Thus, the intensity at x due to a unit point object at X_o may be described as $g(x,X_o) = g(|x - x_o|)$, where $x_o = MX_o$, and if we

---

*This statement must be qualified. The ray $\Sigma_i 0$ will not exist if the line $\Sigma_i 0$ intersects another portion of the object in the point $0'$, where the ray $\Sigma_i 0'$ is unobstructed. If all the rays $\Sigma_1 0, \Sigma_2 0, \ldots, \Sigma_n 0$ are obstructed, then an image of 0 is not formed. This is a phenomenon common to systems which image opaque objects.

weren't aware of the camera's intrinsicly blurred imagery, we would conclude that the object was not a point, but the intensity pattern $G(|X - X_o|)$ $= c\ g\ (M|X - X_o|)$, c a constant.

The function $G(|X - X_o|)$, the apparent shape of the point object, is most important. If the approximate radius of this function is r, then a picture will not resolve two points spaced more closely. Fortunately, $G(|X - X_o|)$ is quite easily calculated. From electromagnetic theory, we know that a unit point source at x_o will give rise to an intensity $\frac{1}{c} G(|X - X_o|)$ on the object plane; this follows from the symmetry of the Green's function. Thus, by placing a point source in the film plane and determining the radiation pattern outside the camera we immediately find the apparent shape into which a point object at a given distance is transformed. Of course this shape depends upon the focal length and pinhole size.

The pinhole camera with a circular aperture may be considered a special case of a camera utilizing a well-corrected lens; a point source on the focal plane produces a wavefront at the aperture which is spherical, i.e. unaberrated. The pinhole does not reconverge the wavefront to a point however, which is analogous to an unfocused camera. Born and Wolf have analyzed the unfocused, well-corrected lens using a Kirchoff integral formulation in which path length differences associated with the spherical waves are approximated by quadratic functions.[8] This approximation is appropriate for the pinhole camera if the points to be imaged are not much closer to the aperture than, say, f/10. (The close range on the other hand is probably governed by geometrical optics.) The exact form of solution is valid only for small field angles.

Born and Wolf's results are reproduced graphically in Fig. 2. The abscissa u is the normalized curvature of the wavefront with respect to a reference sphere centered on the observation point and intersecting the wavefront in the center of the aperture. The ordinate v, to the degree of approximation involved, is the normalized distance of the point of measurement from the center of the radiation pattern, transverse to the optical axis. Only points, say, to the right of the origin are relevant to the pinhole camera. The lines $|v| = u$ are the limits of the geometrical shadow of the aperture cast by the point source on the film plane.

The normalization of the intensity plotted in Fig. 2 is inappropriate for our problem, however. We are interested in the camera's resolving capabilities and to this end in Fig. 3 we plot the approximate width of the radiation pattern. The coordinates are given by

$$u = \frac{2\pi a^2}{\lambda} \left(\frac{1}{d} + \frac{1}{f} \right) , \tag{1}$$

$$\bar{v} = \frac{2\pi}{\lambda} \left(\frac{a}{d} \right) r , \tag{2}$$

where: λ = wavelength of light

a = pinhole radius

f = focal length of camera

d = axial distance of point of measurement from center of pinhole

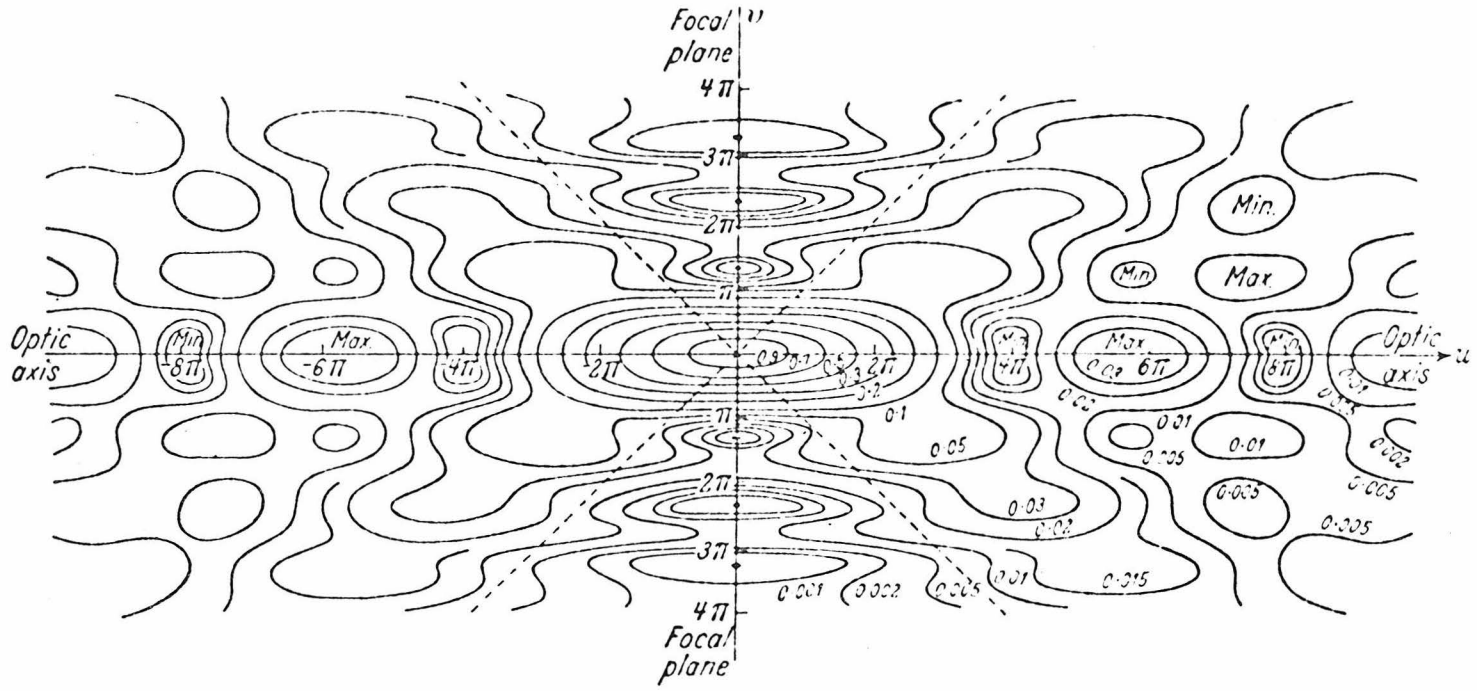

Fig. 2 Isophotes of the three-dimensional light intensity distribution near the focus of a well-corrected lens. The coordinates are normalized axial (u) and transverse (v) dimensions, for source on axis. There is rotational symmetry about the line v = 0. (Adapted from E. H. Linfoot and E. Wolf, Proc. Phys. Soc., B, 69, 823 (1956), and from M. Born and E. Wolf, Principles of Optics (second edition), p. 440, The MacMillan Co., N. Y. (1961)).

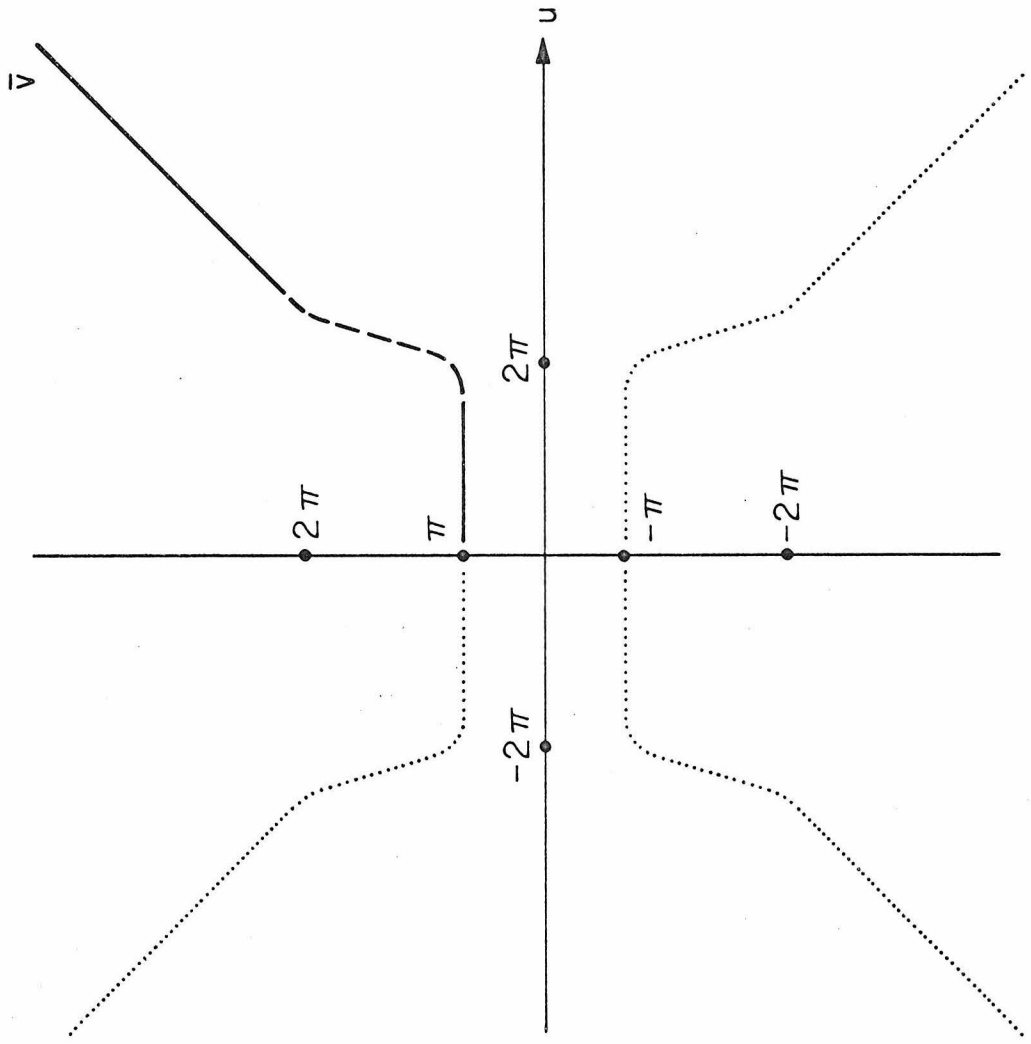

Fig. 3 The approximate width of the radiation pattern of a well-corrected lens or pinhole camera. For paraxial pinhole camera imagery, u is related to the axial distance from the aperture and v to the approximate transverse dimensions of the pattern (see text). (cf. Fig. 2)

r = approximate radius of the pattern measured, in the transverse direction, from the extension of the straight line which connects the point source in the focal plane with the center of the aperture.

Roughly speaking, Fig. 3 may be described by the equations:

$$\bar{v} \simeq \pi, \quad u \lesssim 2\pi \quad , \tag{3}$$

$$\bar{v} \simeq u, \quad u \gtrsim 2 \quad . \tag{4}$$

There is a smooth transition between the two domains in the vicinity of $u = 2\pi$. Equations (3) and (4) may be respectively put into the forms (5) and (6):

$$r \simeq \tfrac{1}{2} \frac{\lambda}{a} d \quad , \quad \frac{\lambda}{a} d > a(1 + \frac{d}{f}) \quad , \tag{5}$$

$$r \simeq a(1 + \frac{d}{f}) \quad , \quad \frac{\lambda}{a} d < a(1 + \frac{d}{f}) \quad . \tag{6}$$

If we are somewhat sloppy with factors of 2, we may thus interpret the radiation pattern as a combination of a geometrical shadow (6) and of a diffraction limited field (5), the net pattern being approximately equal to the larger of the two contributions; in any imaging problem we should optimize (with respect to aperture size) the resolution by balancing the one against the other.*

*We disregard here the possibility of optical spatial filtering (see Section 6.6).

A manifestation of the factor of 2 mentioned above is diffraction focusing. For example, in imaging a plane object at a fixed distance, we may improve the resolution by up to $\sim 30\%$ by using an aperture $\sim 30\%$ greater than that suggested by a geometrical-diffraction balance. In the case of more complicated objects and imaging systems, less than 30% can be gained in this manner.* Diffraction focusing is a phenomenon common to all the optical systems we shall describe, and its small effect should of course be considered in practice. However, we shall neglect it here, for a simple presentation.

Another detail which we shall not consider explicitly in our simplified analysis is the fact that the stereogram requires a two step process, i.e. both imaging and projection. If the same optical system is used for both steps, the spatial impulse response of the entire process is given by the spatial autocorrelation of that of the imaging step. We shall assume that the second step has the effect of increasing the blur by a factor of approximately $\sqrt{2}$, as would be exactly the case for a gaussian impulse response. If in practice diffraction focusing is effectively utilized, it will almost cancel the two-step effect.

2.3 Three-Dimensional Imagery with the Pinhole Camera Stereogram

In stereogram applications of the pinhole camera, $d >> f$. Then the radius of the geometrical shadow, or cue, is $r_g \simeq \frac{a}{f} d$, and that of the diffraction pattern, or cue, is $r_d \simeq \frac{\lambda}{2a} d$. The best aperture radius choice is therefore

*We disregard here the possibility of optical spatial filtering (see Section 6.6).

$$a \cong \left(\frac{\lambda f}{2} \right)^{1/2} , \tag{7}$$

and from substitution into (1) we have

$$u \cong \pi \left(1 + \frac{f}{d}\right) . \tag{8}$$

Except for $d = \infty$, the geometrical cue is then always dominant, if only slightly so. (A slightly larger value of u would be used if diffraction focusing were considered.) As shown in Fig. 4, the resolvable object element is of width ϵ, where

$$\epsilon \cong d\left(\frac{\lambda}{2f} \right)^{1/2} , \tag{9}$$

except for small d, where a is the limit of resolution. Thus, for given f, we have

$$\epsilon > a \cong \frac{1}{2} \frac{\lambda}{\epsilon} d . \tag{10}$$

The maximum d or depth of focus, d_{max}, is given by

$$d_{max} \cong \frac{2\epsilon^2}{\lambda} , \tag{11}$$

where ϵ is the required (maximum) resolution element.* While this value is

*The depth of focus is infinite if we only specify angular resolution (which is related to picture sharpness).

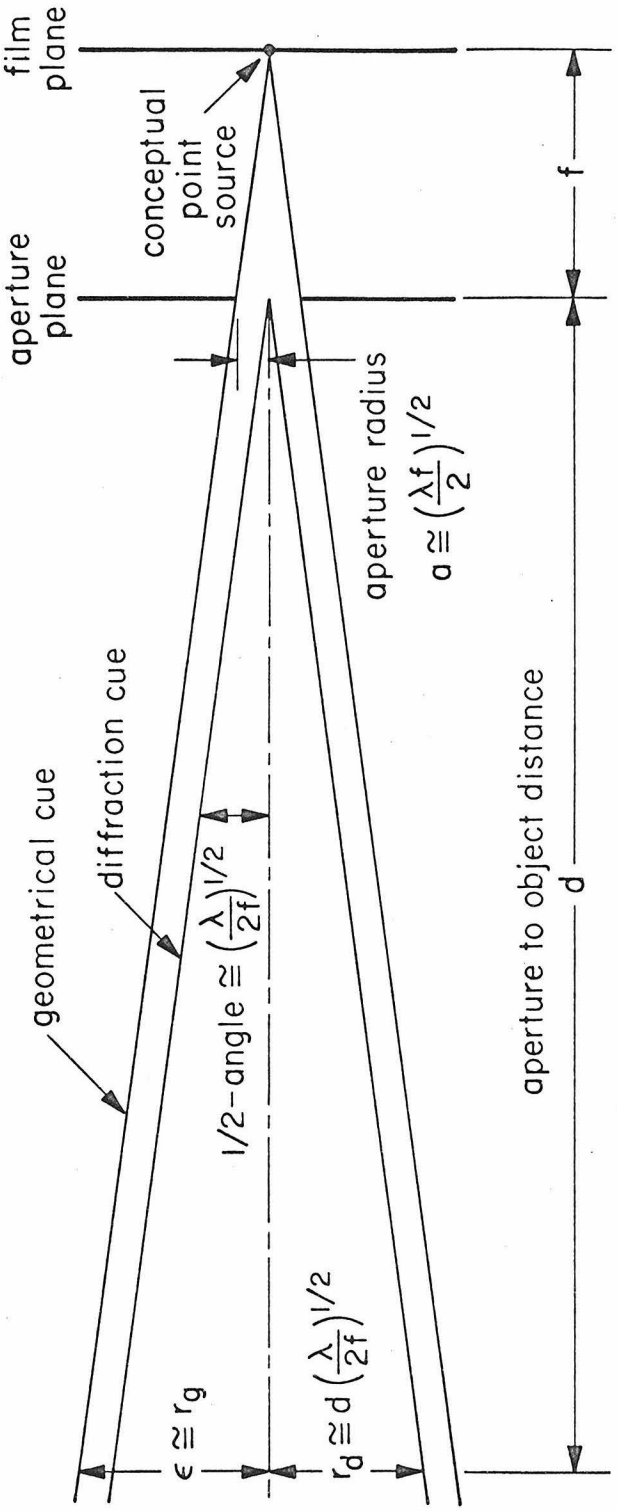

Fig. 4 Determination of the resolution element ϵ for imagery of an object at distance d from an optimized pinhole camera, i.e. in which $a \cong (\lambda f/2)^{1/2}$, for $d \gg f$.

typical of all stereogram systems, we should note that the pinhole camera, unlike the other systems, must be located within this depth of focus region.

The number N of discernible line elements across the picture is approximately equal to the ratio of the spacing s between adjacent pinholes to the aperture radius a.

$$N \cong s/a \quad (a \cong (\frac{\lambda f}{2})^{1/2}) \quad . \tag{12}$$

This is easily seen by noting that the geometrical shadow of the aperture cast onto the film by a point object at $d >> f$ is a circle of approximate radius a, and that the total image size cannot exceed the spacing s. We may define an approximate F number of the cone of rays contributing to a real image point

$$F \cong \frac{1}{2 \tan \psi} \cong \frac{d}{ns} \quad , \tag{13}$$

$$(n \geq 2 \ , \ \psi \cong \tan \psi) \quad ,$$

where n is the number (in one dimension) of apertures contributing, and ψ is the half angle of the cone. Since the aperture radius subtends, from the object, an arc of $\frac{1}{2} \frac{\lambda}{\epsilon}$, we have

$$N \cong (\frac{2\psi}{n})/(\frac{1}{2} \frac{\lambda}{\epsilon}) = \frac{4 \epsilon \psi}{n \lambda} \quad . \tag{14}$$

The half field angle of the camera is obviously approximately equal to ψ , i.e.,

$$\frac{s}{2f} \cong \psi \, . \tag{15}$$

Since the camera cannot function well at extreme angles,

$$\psi \lesssim 1 \, , \tag{16}$$

and from (13) and (16)

$$s \lesssim d \quad (n = 2) \, . \tag{17}$$

Also, note from (13) and (14) that

$$N \lesssim \frac{2\epsilon}{\lambda} \, . \tag{18}$$

For $\psi \cong 1$, the limit of $d \cong s \cong f$ also corresponds roughly to the closest point at which an angular resolution of $\sim \frac{\lambda}{2a}$ is attained (cf. (5) and (6)).

The number of resolvable lines N is significant for the virtual image. But for the real image, since many cameras contribute, n is more important. Since $\frac{\epsilon}{d}$ is the smallest resolvable angle,

$$\frac{\epsilon}{d} = \left(\frac{2\psi}{N} \right) \, . \tag{19}$$

From (10), (14), and (19), we find

$$n \simeq \frac{2}{\lambda} \frac{\epsilon^2}{d} \simeq \frac{\epsilon}{a} \quad . \tag{20}$$

Therefore, if the camera system is designed to be just within the depth of focus of the object (cf. (11)), or just close enough to resolve the line width ϵ, n is of the order of unity. If the camera is designed to be closer, n becomes proportionately larger, at the expense of the useful depth of focus. However, n is independent of the field angle ψ. Equation (14) can be put in the form

$$n \left(\frac{N}{2\psi}\right) \left(\frac{\lambda}{\epsilon}\right) \simeq 2 \quad . \tag{21}$$

Here we see plainly how the relative resolution $\left(\frac{\lambda}{\epsilon}\right)$ determines a real-virtual quality product $n \times \left(\frac{N}{2\psi}\right)$.

The choice of s, the camera spacing which determines the field angle ψ can proceed somewhat independently of the other parameters of the system. For the virtual image, the desirability of a large field angle is balanced against the accompanying increase of "dead space" ratio $(s/a)^2$; in the case of the real image, spreading the n contributing rays over a large angle ψ lends precision to measurements at the expense of the unnatural "dead space" $(s/a)^2$ contained in the image-forming cone.

In conclusion, the pinhole camera must be located within a distance $\sim 2\epsilon^2/\lambda$, or within the depth of focus, of the object. The maximum possible number of resolvable lines N in the picture is $\sim 2\epsilon/\lambda$, where ϵ is the

specified line width. Equally significant is the fact that the cone of rays involved in forming, say, a real image is severely incomplete. The filling ratio in one dimension is approximately $\frac{1}{N}$. The number in one dimension of rays forming the image is given by the inverse of the utilized fraction of the available depth of focus.

CHAPTER THREE

THE FLY'S EYE LENS STEREOGRAM

3.1 Introduction

An improved version of the stereogram, proposed by Lippmann,[9] utilizes a fly's eye lens in place of the pinhole camera array. As the name implies, the fly's eye lens is an array of small lenslets closely packed side-by-side. Each lenslet, comparable in size to the pinholes previously proposed, acts in a similar manner in conjunction with its film plane to reconstruct rays on the fly's eye reference surface. A hexagonal close-packed arrangement may be used, so that the individual lenslets may be considered to be roughly circular in shape.

The fly's eye lens represents two important improvements over the pinhole camera stereogram. The first is the elimination of dead space between adjacent camera apertures. This is accomplished by using a lenslet focal length short enough to compress the size of each picture to a size approximately equal to the lenslet diameter. Thus, adjacent lenslets touch each other and the result is a more natural appearing virtual image which exhibits a relatively small "screen" effect due to the small amount of dead space (near the borders of the lenslets). Also, the cone of rays contributing to a portion of the real image is nearly completely filled out.

The second important advantage of the fly's eye lens arises from the focused geometrical cue – the radiation pattern from a (image) point source on the focal plane is relatively concentrated at the conjugate (object) point. We may thus diminish the diffraction cue, which is analytically identical to that of

the pinhole camera, by increasing the camera aperture, without compromising the geometrical cue radius at the conjugate point. As a result, we need not restrict the camera location to within the depth of focus of the object field, i.e. to within $\sim 4\epsilon^2/\lambda$ where ϵ is the required resolution. The region of object space within which resolution of ϵ can be attained is however always limited to depth $\sim 4\epsilon^2/\lambda$.

However, presently available fly's eye lenses are constrained by technology to rather simple design and for this reason are subject to severe aberrations. These aberrations can be controlled, but at the expense of the field angle, (or ray cone angle), which is therefore usually quite small.

The fly's eye lens has previously been analyzed by Burckhardt,[10] but aberrations were neglected in that treatment.

3.2 The Focus Cue and General Photographic Applications

In Fig. 5 is shown the diffraction cue and geometrical, or focus cue for a perfect (aberrationless) lens. These may be derived, as for the pinhole camera, by assuming symmetry of the scalar Green's function and determining the far field radiation pattern resulting from a point source in the film plane. This source yields a converging spherical wavefront immediately outside the camera, centered upon the conjugate point.

In the far field the diffraction cue is a cone axially aligned with the source's conjugate point, with vertex in the center of the entrance aperture, whose half-angle of divergence is $\sim \frac{\lambda}{2a}$, where a is the lens radius. This is the locus of points whose Kirchhoff integral contributions

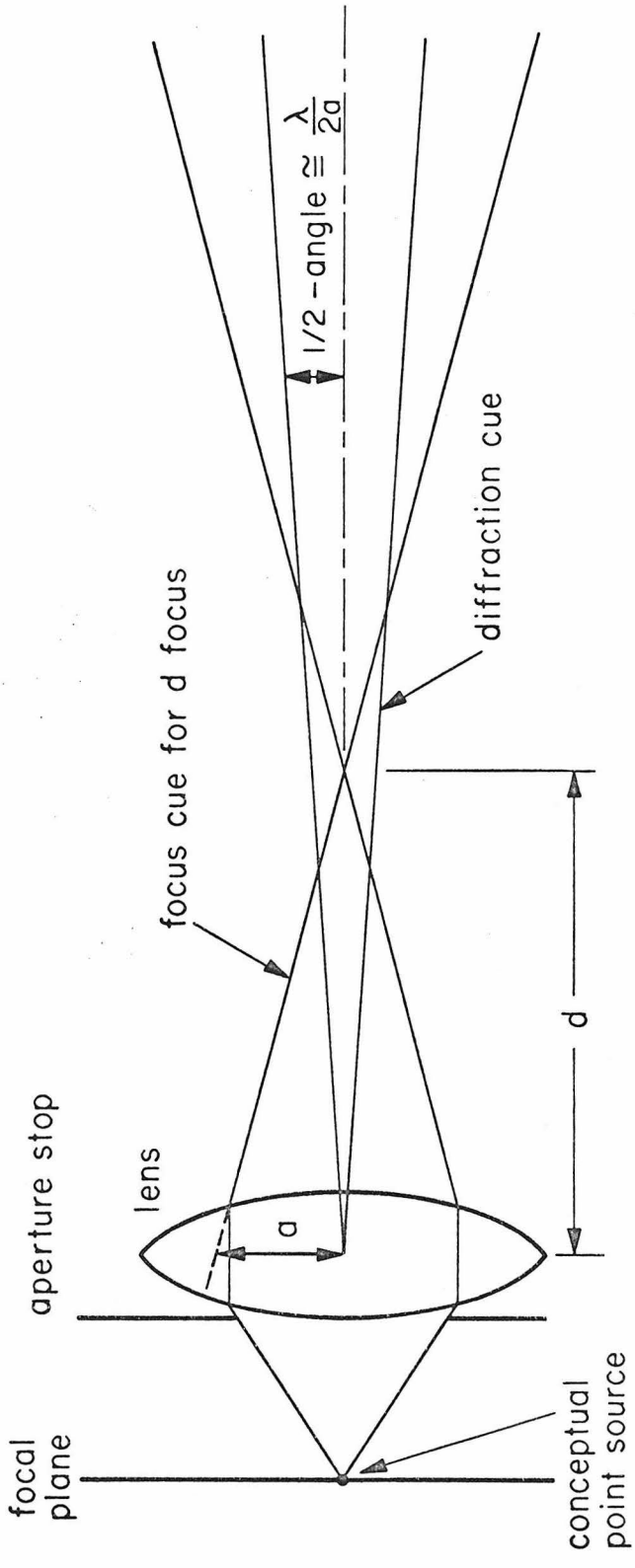

Fig. 5 Illustrating the diffraction and focus cues for a lens of effective aperture radius a focused at a distance d.

from extreme opposite portions of the spherical wavefront in the associated tangential plane of the aperture differ in phase by approximately 2π.

The focus cue is a double cone which intersects the entrance aperture circumference and whose vertex is at the conjugate, or object point of focus. This is the locus of points for which the stationary phase part of the Kirchhoff integral arises from portions of the spherical wavefront on and near to the aperture edge. Simply stated, the focus cue is the boundary of the geometrical shadow of the aperture cast by a point source in the focal plane.

The cues are interpreted the same way as for the pinhole camera. The apparent shape into which an object point at any distance is transformed under imaging is a blur of dimensions approximately equal to the cross section of the larger of the cues at that distance. We must also include in our considerations a third cue, that due to aberrations. The cues are not additive in any strict sense – we merely determine which is dominant for a given situation.

In general our resolution criteria may vary throughout the object space, and it is best to proceed in an ad hoc manner. However, two cases of special interest are presented here. The first is of interest for scenic photography – a simple method is given for visualizing the hyperfocal distance. The second case often arises in the process of almost – perfect imagery.

In ordinary photographic work, the lens-film system is typically designed for relatively high speed. The compromises involved in the design of the lens leads to aberrations, and high speed films are limited in their resolving capabilities. For example, suppose we use a 2 inch lens with a resolution of about 70 lines/mm. with a film whose modulation transfer function cuts off near 70 lines/mm.. Convolving the response of the film with that of the lens yields a

resolution of approximately 50 lines/mm. or 1/2500 radian. Suppose the lens is set at f/2 and focused at infinity. The focus cue is then a 1/2 inch radius cylinder extending to infinity, and beyond 1250 inches the associated blurring is less than 1/2500 radian – hence objects beyond 1250 inches cannot be imaged any more sharply by more careful focusing. However, by focusing the lens at 1250 inches, the hyperfocal distance, objects from half this distance to infinity are resolved with resolution of 1/2500 radian. A graphical interpretation of the hyperfocal distance for the general case is given in Fig. 6.

3.3 Choosing Parameters for the Fly's Eye Lens

Lenses for stereogram applications are frequently diffraction-limited, and under appropriate circumstances aberrations may be neglected. Furthermore, high resolution films are used when necessary, so film associated image degradations are often negligible.* The analysis may therefore proceed similarly to that for the pinhole camera, as a balance between the diffraction and focus cues.

Suppose we specify ε, the width of an object element to be resolved, constant throughout some depth L of object space. Then, since the focus cue is symmetrical with respect to the object plane of focus, we may minimize the "worst" radius of the cue by focusing at a distance midway into the object depth L. The half angle α of the focus cue is given by

*No optical system is capable of resolving an element smaller than the wavelength of light, and there are films which can do approximately this well, e.g. Kodak 649F.

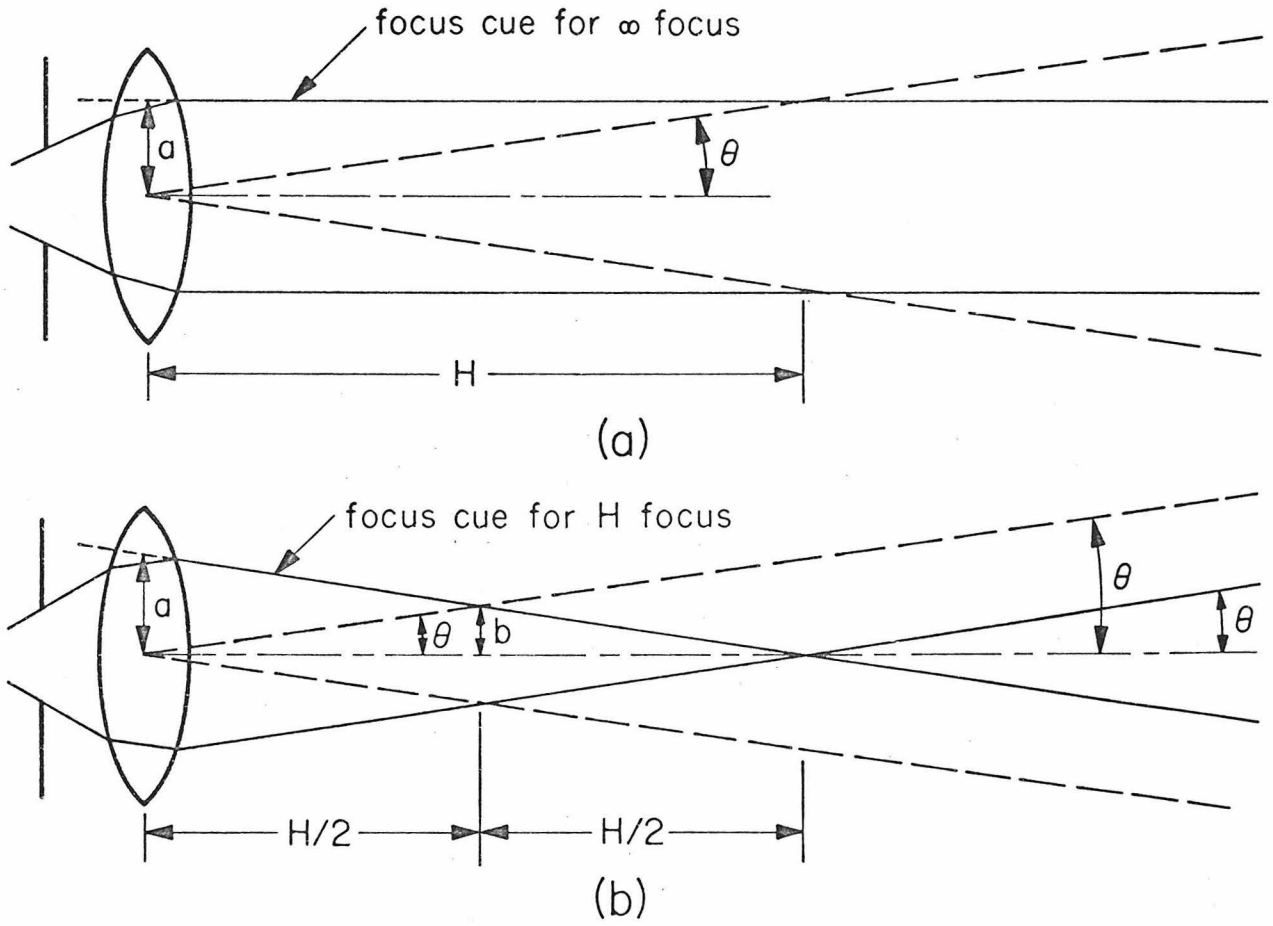

Fig. 6 (a) Determination of hyperfocal distance H based on desired angular resolution θ and lens radius a, using the focus cue for ∞ focus.
(b) With lens focused at hyperfocal distance, depth of focus extends from half-hyperfocal distance to infinity. Degree of blurring, radius b, at H/2 corresponds to same angular resolution θ as at infinity.

$$\alpha = a/d \quad , \tag{22}$$

where d is the distance from the focused plane to the camera. The radius of the diffraction cue at the midplane of the object is

$$r_d = \frac{\lambda d}{2a} = \frac{\lambda}{2\alpha} . \tag{23}$$

If the camera to object distance d is considerably larger than the object depth L, we may consider r_d to be essentially constant. We may arrange for this condition to exist by increasing d, and also a in proportion – thus keeping α, the significant parameter, fixed. In this way, the diffraction cue tends toward a cylinder. Not only is computation simplified, but a better balance against the focus cue is possible since the diffraction cue acquires approximate symmetry about the plane of focus. The worst focus blur is $(\frac{L}{2})\alpha$; the best balance against diffraction, $\lambda/2\alpha$, occurs for

$$\alpha = (\frac{\lambda}{L})^{1/2} \quad , \tag{24}$$

$$\epsilon = (\frac{L}{2})\alpha = \frac{1}{2}(L\lambda)^{1/2} . \tag{25}$$

The camera-object distance d, as was suggested earlier, is relatively unimportant. Notice however that the depth of focus is

$$L = \frac{4\epsilon^2}{\lambda} \quad , \tag{26}$$

just twice that of the pinhole camera. Alternatively, if we wish to image with the best possible angular resolution an object extending from d to infinity, we again balance the focus and diffraction cues. By referring to Fig. 6 we find that the angular resolution $\omega_{\infty f}$ determined by the focus cue is

$$\omega_{\infty f} = \frac{a}{2d} , \tag{27}$$

while that of the diffraction cue is

$$\omega_{\infty d} = \frac{\lambda}{2a} . \tag{28}$$

The best resolution occurs for

$$a = (\lambda d)^{1/2} , \tag{29}$$

$$\omega_{\infty f} = \omega_{\infty d} = \tfrac{1}{2}\left(\frac{\lambda}{d}\right)^{1/2} . \tag{30}$$

Notice that the resolution element ϵ_d at distance d is

$$\epsilon_d = \frac{a}{2} , \tag{31}$$

and

$$d = \frac{4\epsilon_d^2}{\lambda} , \tag{32}$$

which is analogous to (26).

3.4 Aberrations of the Fly's Eye Lenslet

It is our purpose in this section to determine, first, under what conditions the degrading effects of aberrations are negligible, and second, what these effects are when aberrations are dominant in the fly's eye stereogram. But the matter of aberrations is not as straightforward as focus and diffraction cues, and some preliminary remarks are in order.

Unlike the previously considered blurring phenomena, aberrations depend upon the details of the lens design. So many parameters and economic considerations are involved in the pursuit of an "optimum" lens, however, that we will probably never find it, nor know how good it might be. Our approach will be based upon some arbitrary but reasonable assumptions which closely follow Lippman's proposals. Each lenslet is assumed comprised of a single element – the film emulsion contacts the back surface of the lenslet, and hence the front of the lens is the only refracting surface. This assumption is based upon the technical limitations of fabricating small lenses, and also upon economics. The front lens surface is spherical, though a better situation might be achieved with aspheric optics at increased expense. In theory at least, the spherical shape permits the use of self correcting methods of polishing – in any case, we consider the refracting surface to be perfectly shaped and polished. The back (emulsion) surface may be curved to minimize the effects of field curvature. Glass of index 1.5 will be assumed, and we shall assume quasi-monochromatic illumination, so that color effects are negligible.

Since adjacent lenslets touch each other, and because aberrations generally decrease with decreasing numerical aperture (N.A.), it is advantageous

to use a sufficiently long focal length to cause adjacent pictures to just touch.* Assuming fairly small field angles, the lenslet F number is equal to the inverse of the total field angle

$$F = \frac{1}{2(\text{N.A.})} = \frac{1}{2\psi} \quad , \tag{33}$$

where ψ is the half-field angle. Then aside from the curvature of the back of the lens, which affects only the field curvature and is of minor overall importance, there are only two independent parameters, e.g. the lens diameter and field angle. We also recall that angular aberrations are independent of a scaling of the optical system, and hence depend only upon the maximum field angle in a well-designed fly's eye lens.

Mathematical modeling of the aberration blurring presents further difficulties. The first, of describing the wavefront emergent from the refracting surface, is easily dispensed with. We assume that the wavefront and ray trajectories are adequately described in terms of the third order Seidel aberrations which are the lowest order terms of an expansion of the wavefront phase in powers of the field angle and of the aperture coordinates. These low order

---

*If the conjugate distances become comparable in magnitude, as for extremely long focal lengths, aberrations increase; as will be shown, however, this is a pathological case which seldom if ever arises (cf. Section 3.5). An increase in F number may be thought by the reader to necessitate a longer exposure time. However, the accompanying expansion of the picture permits the use of faster, lower resolution film. We require interception of a given number of photons from each resolution element (depending upon signal to noise requirements). Only the lens diameter and film quantum efficiency of absorption are important for this.

terms, which would be balanced against higher order terms in a complex and well-designed lens, are dominant in our simple lens for moderate values of field angle and numerical aperture.

We have seen that the focus cue is essentially the geometrical shadow of the aperture, and as such has a well-defined width. The diffraction cue being merely a slight extrapolation in three dimensions of the Airy pattern also has a fairly well-defined width of well-known dependence upon physical parameters. The shapes of aberration spots, however, are much more complex, and their widths are thus more difficult to pin down analytically. Neither is there a simple relation between spot size and resolution – the dependence of aberrations upon field angle suggests a non-spatially-invariant optical system to which the application of modulation transfer function (M.T.F.) concepts is not strictly valid. We shall assume, however, that an M.T.F. could be defined, if only over sufficiently localized portions of the field.

A commonly used method for visualization of the Seidel aberrations is to plot the locus of intersections with the focal plane of rays originating from various radii of the aperture, as a function of field angle, using geometrical optics. If we try to extend this technique slightly, to determine the intensity within the spot by adding coherently or incoherently the contributions from the various rays, trouble arises in the form of singularities. These are only apparent, however; as will be shown in Section 4.5, the (spatial) spectrum of the spot is band limited.

By using a more satisfactory treatment based on the diffraction theory of aberrations we would not find these singularities, but this is unnecessarily complicated for our purposes. In our treatment, the geometrical theory of

aberrations is used in a way typical in optical design work* – we estimate the radius of the smallest circle into which the rays from a reasonable percentage, say 80%, of the total aperture fall. The sum of such radii calculated from each primary aberration coefficient separately is often taken as a conservative (large) estimate of the total aberration blurring; we use a root of sum of squares value. The smallest circle through which 100% of the rays pass is not located in the gaussian focal plane, and its radius is typically of the order of 1/3 the distance from the gaussian image point to the intersection with the focal plane of the rays from the extreme portions of the lens; the smallest circle through which 80% of the rays pass, however, is closer to the focal plane and smaller by a factor of the order of 1/3.[11] Therefore, somewhat arbitrarily, we shall use as an estimate of the blurring of each aberration a disc of radius 1/9 the distance of the extreme ray from the gaussian image point.

For moderately small N. A., the plane of the apices of the fly's eye lenslets may be taken as the aperture stop position. With this assumption, the primary aberrations may be calculated in a straightforward manner (see Appendix I), and a cue associated with each of the aberrations may be drawn with vertex in the lenslet aperture. The half-angle of divergence of each of the cues is given in Table 1. These values are for the "worst case", both with respect to contributing rays and field position. Distortion is not considered because it is cancelled in the two step process. Several values (0, ¼, ½) of γ, the ratio of

---

*This approach is most appropriate for spherical aberration. It will be shown that this is the dominant aberration (cf. Tables 1,2).

the respective distances from the lens apex to the conjugate points, are included. For most stereogram applications, $\gamma << 1$.

In Table 2 the aberrations are given for a well-designed fly's eye lens, i.e. N.A. = ψ. The values here include the above referred to factor of 1/9 as well as a factor of $\sqrt{2}$ to account for the two step nature of stereogram imagery. Also given is the root of the sum of the squares of the individual aberrations, which we shall take as representative of the total aberration blurring. This angular blur is given by $\beta(\gamma)\psi^3$. For almost all interesting cases $\gamma << 1$, and $\beta \cong 0.16$.

Suppose we have an object of transverse dimension h, longitudinal depth L, at an approximate distance d from the lens array, and $d \gtrsim L$. The depth of focus and diffraction limit the angular resolution ω_{oL} to (cf. (25))

$$\omega_{oL} = \frac{\epsilon}{d} \cong \frac{(L\lambda)^{1/2}}{2d} , \tag{34}$$

if ϵ is minimized with respect to lens diameter and focus. However, since $\psi \cong \frac{h}{2d}$, we are limited by aberrations to angular resolution ω_a of

$$\omega_a = \beta \psi^3 = \frac{\beta}{8} \frac{h^3}{d^3} . \tag{35}$$

Comparing the two, we have

n = 1.5	General Form	$\gamma = \frac{1}{2}$	$\gamma = \frac{1}{4}$	$\gamma = 0$
spherical	$\frac{(1+\gamma)^2 (1+n)}{2n^2 (n-1)^2} (N.A.)^3$	$3.50\ (N.A.)^3$	$1.91\ (N.A.)^3$	$0.89\ (N.A.)^3$
coma	$\frac{(1+\gamma)(1+\gamma n)}{2n^2 (n-1)} (N.A.)^2 \psi$	$1.17\ (N.A.)^2 \psi$	$0.76\ (N.A.)^2 \psi$	$0.44\ (N.A.)^2 \psi$
astigmatism	$\frac{(1+\gamma n)}{2n^2} (N.A.) \psi^2$	$0.39\ (N.A.) \psi^2$	$0.31\ (N.A.) \psi^2$	$0.22\ (N.A.) \psi^2$

TABLE 1. Half-angle of divergence of aberration cues, taken separately, of lens with single refracting surface. The values are for "worst case" both with respect to contributing rays and field position where applicable. Circle of least confusion is basis for value given for astigmatism, which implies that field curvature is compensated for by shaping of the back (emulsion) surface of the lenslet. Ratio of image, object distances from lens apex is γ.

	$\gamma = \frac{1}{2}$	$\gamma = \frac{1}{4}$	$\gamma = 0$
spherical	$0.55\ \psi^3$	$0.30\ \psi^3$	$0.140\ \psi^3$
coma	$0.18\ \psi^3$	$0.12\ \psi^3$	$0.070\ \psi^3$
astigmatism	$0.06\ \psi^3$	$0.05\ \psi^3$	$0.035\ \psi^3$
$\omega_a = \beta(\gamma)\psi^3$ (r.s.s.)	$0.58\ \psi^3$	$0.33\ \psi^3$	$0.16\ \psi^3$

TABLE 2. Half-angle of divergence of aberration cues of lens with single refracting surface, of $\sqrt{2}/9$, for ψ = N.A. Values given for each aberration separately, and for square root of sum of square root of sum of squares (r.s.s.) which represents total angular blur $\omega_a = \beta(\gamma)\psi^3$.

$$\frac{\omega_a}{\omega_{oL}} \simeq \frac{\beta}{4} \left(\frac{h}{d}\right)^2 \left(\frac{h}{L}\right)^{1/2} \left(\frac{h}{\lambda}\right)^{1/2}$$

$$\simeq 0.04 \left(\frac{h}{d}\right)^2 \left(\frac{h}{L}\right)^{1/2} \left(\frac{h}{\lambda}\right)^{1/2} . \qquad (36)$$

Alternatively, if we consider an object extending from d to infinity, of half-field angle ψ, we focus on the hyperfocal distance and

$$\omega_{o\infty} = \tfrac{1}{2} \left(\frac{\lambda}{d}\right)^{1/2} , \qquad (37)$$

$$\frac{\omega_a}{\omega_{o\infty}} \simeq 0.04 \, (2\psi)^3 \left(\frac{d}{\lambda}\right)^{1/2} , \qquad (38)$$

where $\omega_{o\infty}$ is the angular resolution in the absence of aberrations.

The ratio ω_a / ω_{oL} becomes worse (larger) as the size of the scene increases, but can be decreased by backing the lenslets away from the object so as to decrease the (full) field of view h/d. For example, an object of dimensions h = L = 10 cm. at distance d = 10 cm. yields $\omega_a / \omega_{oL} \simeq 18$. By pulling back to about 42 cm., this can be decreased to unity, with full field of 13^o. As another example, a scene extending from 1 meter to infinity yields $\omega_a / \omega_{o\infty} \simeq 2.4$ for a full field of 20^o, $\omega_a / \omega_{o\infty} \simeq 19$ for 40^o.

Clearly, aberrations limit the performance of the fly's eye lens in many typical applications, particularly where wide angle fields are desired.

In addition to aberrations, the fly's eye lens is subject to several other problems. First is the matter of film registration – a slight shrinkage of the emulsion might have a severe cumulative effect across the full width of the array of lenslets. Another problem is that the 3–D image is pseudoscopic. This can be overcome by using yet another fly's eye array to invert the image back to an orthoscopic one by making a second stereogram of the image of the first one, as proposed by Lippmann. Of course, this results in further degradation of the image quality.

R. V. Pole utilized the principle of holographic wavefront reconstruction to reverse to orthoscopic the fly's eye image.[12] The holographic step here replaces Lippmann's second stereogram and has the advantage that the amount of image degradation introduced is negligible. Other problems arise, however. The first stereogram must be projected with coherent light, and a coherent reference beam must also strike the hologram plate. In practice, this has meant that the hologram plate must be separated by a considerable distance from the fly's eye lens, which has the unfortunate result that the viewer of the resulting hologram seems to look through the "tunnel" formed by the hologram and (image of) the fly's eye lens – the result of this is a further restriction upon the angle of view.

The fly's eye lens seems to be a promising method of 3–D imagery if the technical limitations are overcome. In particular, the author believes that much improvement is possible by applying holographic methods. For example, it may be possible to synthesize holographic lenslets which are as well corrected for aberrations as multi-element lens systems.

3.5 Comparison of Stereogram Imagery with Ordinary Photography

It was noted above that $\gamma << 1$ for most cases. It is simple to show that the number n of fly's eye lenslets (in one dimension) contributing to, say, a real image point is given by

$$n \cong \frac{1}{\gamma} \quad . \tag{39}$$

Thus, if γ becomes comparable to unity, n becomes quite small and one can then hardly refer to the result as a stereogram.

We might ask what is gained by making n large. Suppose we take an ordinary photograph of an object, with a focus cue of half-angle α. The resolution element is $\epsilon = \lambda/2\alpha$, and the depth of focus $L = \lambda/2\alpha^2$ (cf. (20), (21)).

If we replace the camera with a fly's eye system of m x m lenslets, the focus cue will have half-angle α/m. The resolution element becomes $\epsilon = m\lambda/2\alpha$. The depth of focus is $L = m^2\lambda/2\alpha^2$ with respect to an individual ray, or lenslet. But the blur which arises in the real image when we move from the correct position is due to the m lenslets (in one direction) and the blurring is m times worse. Therefore the longitudinal resolution element is L/m or $m\lambda/2\alpha^2$, and there are m resolvable elements of depth. Thus, while the linear size of the resolution element increases in both the transverse and longitudinal directions by the factor m, we gain a factor of m in the number of elements in the longitudinal direction. But the number of resolvable elements of volume decreases by m. The fly's eye lens is of

course subject to aberrations which further decrease the number of elements, though, as we shall see, the holographic stereogram overcomes this problem.

CHAPTER FOUR

THE HOLOGRAPHIC STEREOGRAM

4.1 Introduction

An alternative approach to the fly's eye lens is the holographic stereogram. The focus cue and diffraction cue are the same as for the fly's eye lens, but aberrations are negligible. Also, an orthoscopic image is obtained directly without any tunnel effect. The price paid for these advantages, and others which will be discussed later, is that the process is inherently slower. The component photographs of the fly's eye stereogram may be taken simultaneously, while those of the holographic stereogram must be taken sequentially (cf. Section 6.1).

Within the Seidel approximation, astigmatism is proportional to the N.A., coma to $(\text{N.A.})^2$, spherical aberration to $(\text{N.A.})^3$. A straightforward method to reduce the aberrations therefore is to reduce the N.A.. We have seen that the N.A. of the fly's eye lenslet cannot be made smaller than the half-field angle ψ, in order that adjacent component photographs not overlap. The restriction against image overlap however, is based upon classical concepts of image deposition onto films – we assume that a double exposure, as it were, cannot in general be resolved back into its components. Of course, this restriction can be overcome with holography. Under appropriate illumination for projection of the 3–D image, each of the component photographs, regardless of overlap, may be made to reconstruct rays which traverse only its respective lenslet. Even with a simple lens, therefore, we may arbitrarily decrease the N.A. and the aberrations by increasing the focal

length. But this approach based upon the fly's eye lens is unnecessarily restrained, and it is interesting to take a more general approach.

4.2 Description of the Holographic Stereogram Process*

The method of the holographic stereogram involves two steps. In the first step, a sequence of ordinary photographs is taken of the incoherently illuminated object, providing a stereoscopic record. Each photograph is taken from a different segment of a reference plane. In the second step, a holographic transformation of each photograph is recorded on the corresponding segment of a hologram plate which is placed in the reference plane. This requires a laser and other appropriate holographic equipment.

For clarity, we shall first consider a very simple form of implementation. Fig. 7 illustrates the taking of a typical photograph from a segment of the observation plane $z = z_{ob}$; a mask is placed in this plane with a pinhole aperture centered at P_a . Behind the mask and aligned with the aperture are placed a well-corrected convex lens and a sheet of photographic film. The lens-film system is focused to record the image, at P_i, of the object-point P_o. For convenience the aperture diaphragm has been placed in front of the lens** in order to be physically accessible as a light mask in step 2.

Just as in the case of the fly's eye lens, the focus cue and diffraction cue effect the resolution, and are determined by the aperture size. Except for

---

*For additional description, see Appendix II.

**See Section 6.2 for other cases.

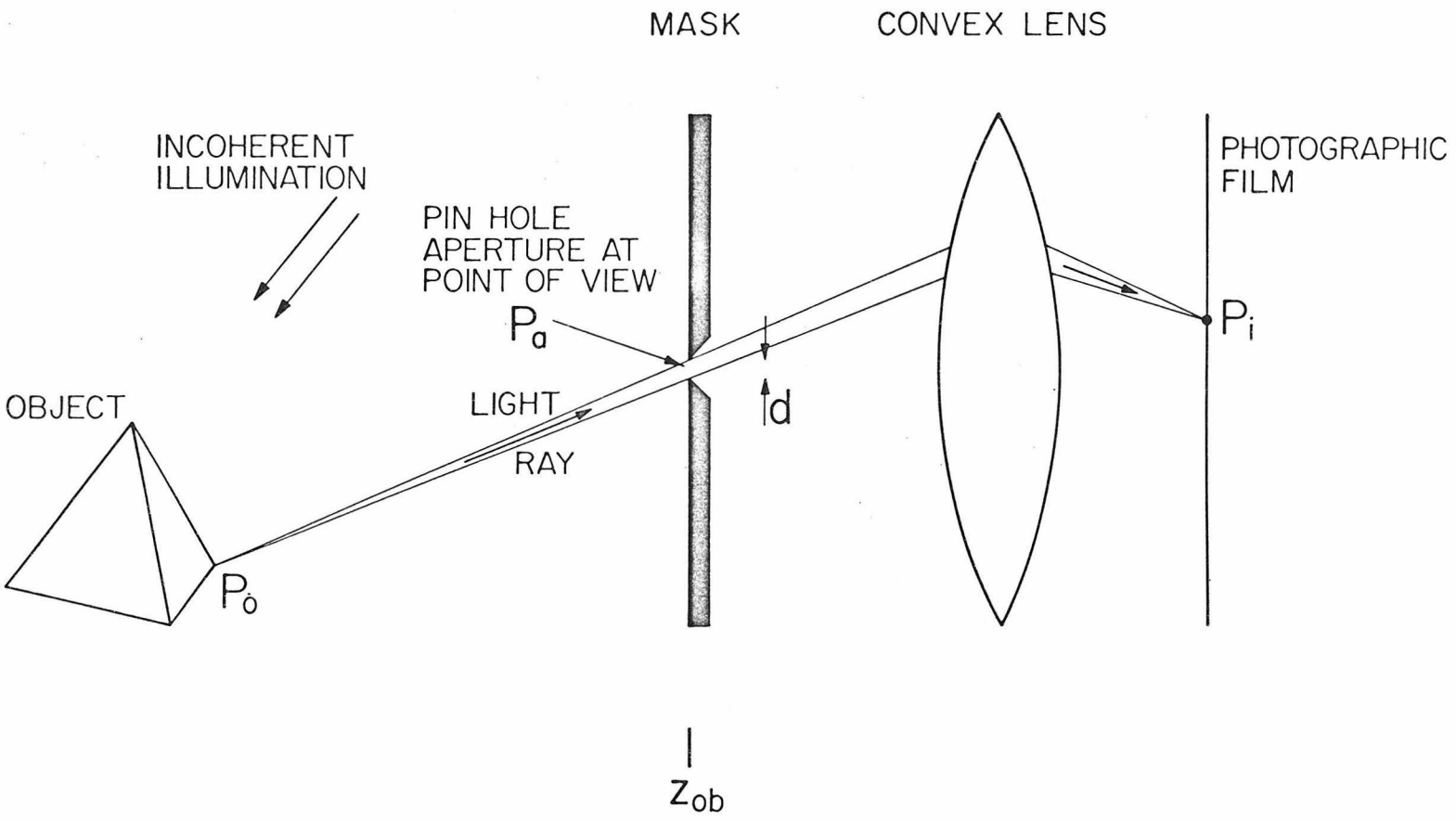

Fig. 7 Taking a typical photograph through pinhole aperture in the plane $z = z_{ob}$, for the holographic stereogram. (Lens-film-pinhole system shown in exaggerated scale.)

distortion, which is inconsequential, aberrations are negligible since the lens is well corrected and used at small N.A. (see Sections 4.3, 4.4).

The film is processed and returned to the original position. As shown in Fig. 8, a coherent plane wave is beamed through an auxiliary lens, at z_c, onto the transparency. The position of this lens, z_c, is adjusted to concentrate the light energy onto the pinhole. If the aperture is placed in the front focal plane of the camera lens, no auxiliary lens is required; if a larger or smaller separation is used, a concave or convex lens is required, respectively. (The result is that, within a phase factor which moreover is negligible for objects well within the depth of focus, the electric field across the plane of the aperture is equal to the Fourier transform of the amplitude transmittance of the photographic image if moderate field angles are used.) Illumination of the image point P_i will cause a light ray to propagate through the small aperture to the object point P_o. We may, as shown in Fig. 8, interrupt this ray with a high-resolution photographic plate, immediately to the left of the aperture. When the image point is coherently illuminated, and the aperture additionally illuminated with a coherent reference beam, at an angle θ, the ray is holographically recorded at the point P_a of the high resolution plate. The object is not present in this step.

If one were to view this hologram, the normal illumination for the two-beam configuration of Leith and Upatnieks is used,[13] i.e. a coherent plane wave is beamed onto the plate at angle θ, as shown in Fig. 9; the reconstructed ray emanates from P_a to the point P_o. The sensitivity of the reconstruction with θ is small, as described in the literature.[14]

The entire process may be repeated at point P_a' on the high-resolution plate, after translating pinhole, lens, and all, to align the system along P_a'.

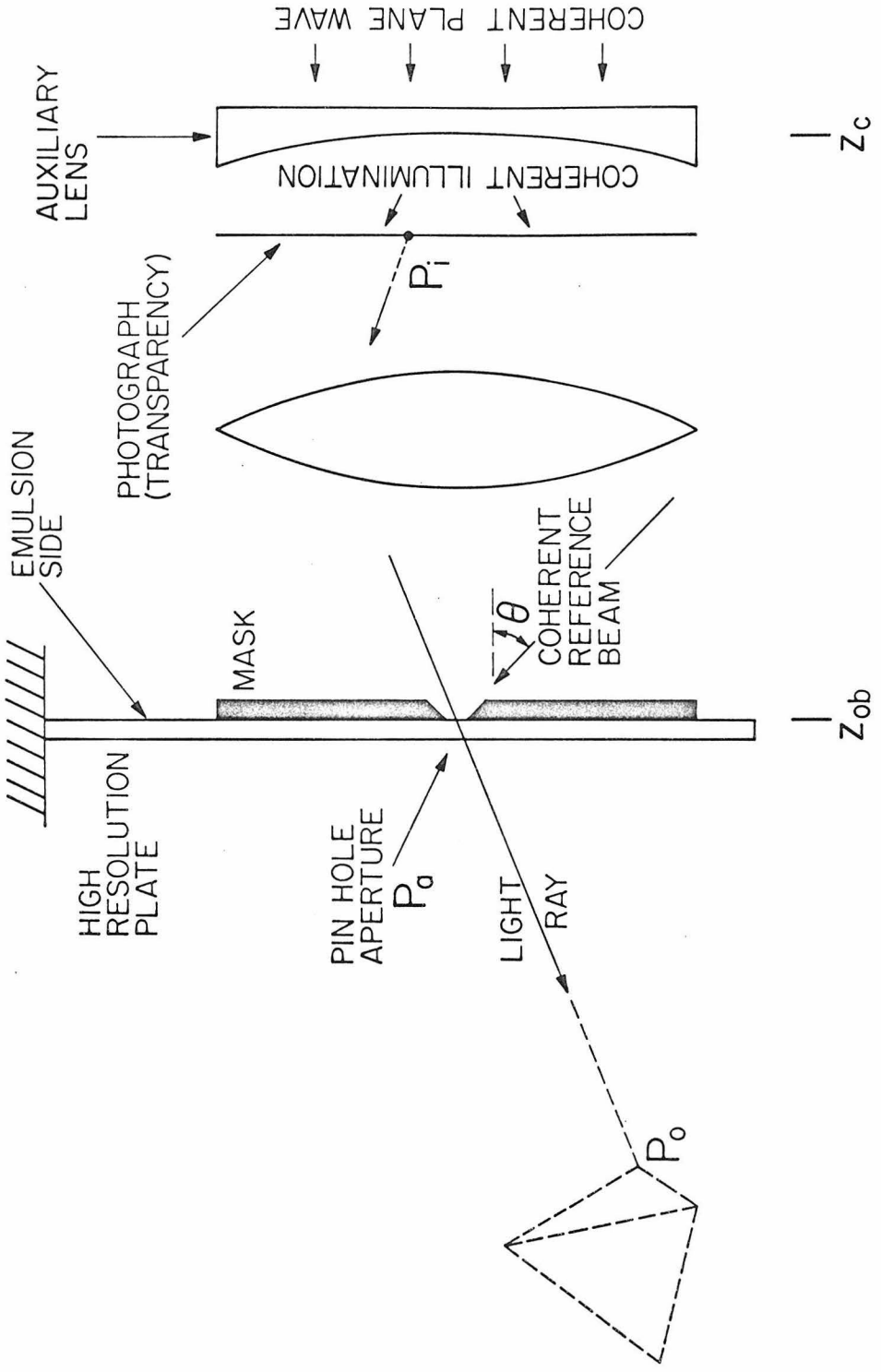

Fig. 8 Synthesis of holographic stereogram on high-resolution photographic plate.

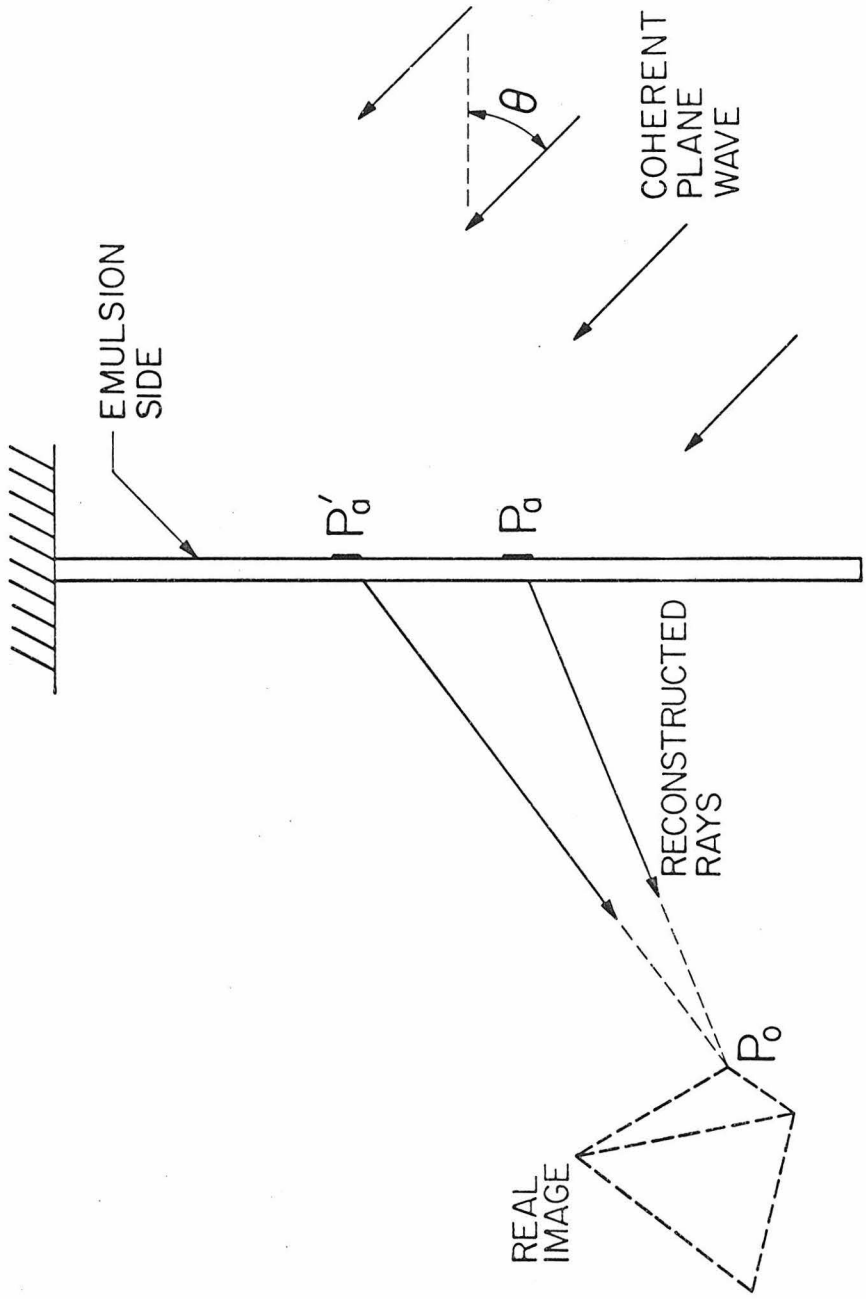

Fig. 9 Holographic wavefront reconstruction of pseudoscopic real image of holographic stereogram.

Fresh film is used to take the corresponding photograph. As shown in Fig. 9, the coherent plane wave illumination will then also result in a ray propagating toward P_o from the point P'_a on the plate.

The process is repeated for all points of a two-dimensional lattice on the high-resolution plate. When the developed plate is plane wave illuminated, the many rays converging at the point P_o will form an observable pseudoscopic real image there, of the object point. All object points are reconstructed this way. If we illuminate the developed plate from the opposite direction, the orthoscopic virtual image is observed almost trivially.

4.3 The Wild Eyepiece as a Holographic Stereogram Camera

While it is possible in theory to completely eliminate aberrations from the holographic stereogram, it is of interest to determine how nearly we may approach this limit in a practical system. We shall consider the use of a wide angle eyepiece as the main component of the camera lens. The use of an eyepiece is suggested by the convenience noted above of having the aperture stop located external to the lens elements, which of course is a feature peculiar to eyepieces. For our application, the aperture stop or pinhole is placed in the plane normally used for the eye position.

A good eyepiece is not necessarily the optimum lens for stereogram applications. Several eyepiece design criteria are of no importance for our use, and the additional flexibility which would be introduced if the constraints imposed by these criteria were relaxed would presumably yield a better lens. In particular, distortion is irrelevant to the operation of the lens, as has been noted.

Since the holograms are formed by monochromatic light, we may also eliminate the effects of chromatic aberrations by using a band-pass filter in taking the component photographs. Spherical aberration and coma, which depend strongly on the N.A. are also negligible since we usually use a very small N.A.. Even in normal operation where the eye pupil acts as the limiting aperture of the eye-piece, a small N.A. is encountered; however, typical eyepiece designs allow for considerable movement of the eye (transverse and lateral) and we do not require this feature. Furthermore, the eye relief may be reduced considerably but subject to the necessity of introducing the reference beam. And if an imaged zone plate reference beam arrangement is used (cf. Section 5.2), the eye relief may be completely eliminated. With the flexibilities thereby introduced, it should be possible to build extremely wide angle objectives with a minimum of field curvature and astigmatism. These two aberrations (usually taken together as a single aberration) remain as the most serious when we use a standard eyepiece as our objective.

In Fig. 10 is given the design data for a Wild eyepiece. The aberrations are given in Figs. 11 and 12 for an eyepiece of this design of 1 inch focal length. We can decrease the aberrations by choosing a longer focal length, but for the moment we consider this particular lens.

As expected, we find that field curvature is dominant for small apertures (diameter $< .3$ cm.). The sagittal image surface has greater curvature than the tangential image surface, leading us to expect that the skew rays will intersect the focal plane with a greater deviation from the Gaussian image point than the meridional rays. This is confirmed from examination of Fig. 11. A very good fit to these data is gotten by using the expression

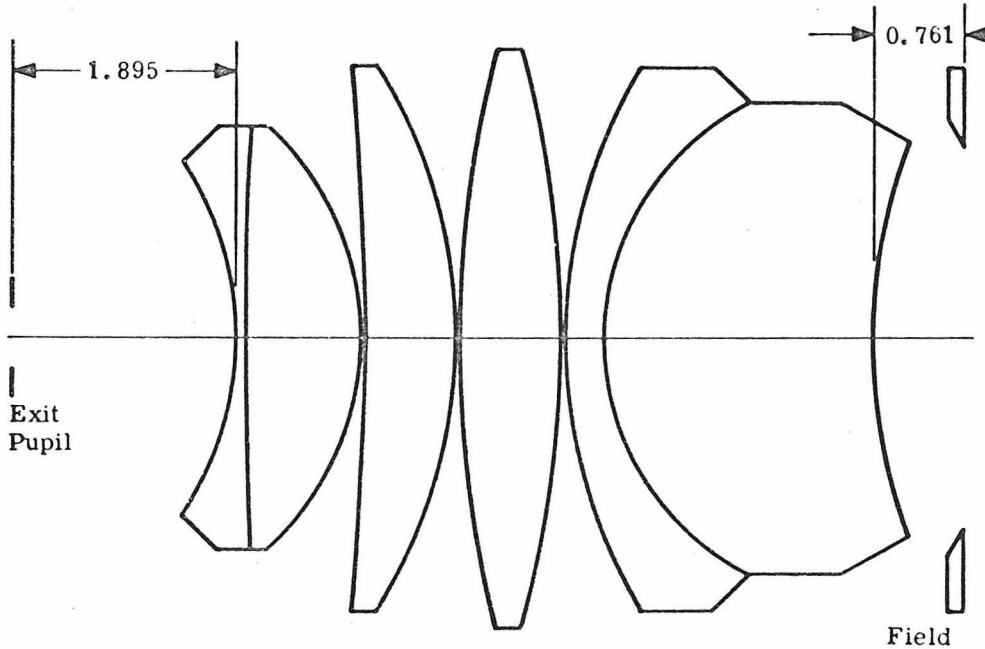

c	t	Glass Type
-0.3636		
	0.10	689309
0.04		
	0.95	620603
-0.4000		
	0.01	Air(n= 1)
-0.0200		
	0.80	620603
-0.2243		
	0.01	Air(n= 1)
0.1025		
	0.85	620603
-0.1025		
	0.01	Air(n= 1)
0.2171		
	0.35	649338
0.4400		
	2.25	573425
0.2170		
	0.761	
$\Sigma P = -0.1538$		
$\gamma = 2.56$		

Table - Lens constants for the Wild eyepiece. Lengths in cm.

Fig. 10 Design data for the Wild eyepiece of one inch focal length. The Petzval sum ΣP and surface curvatures c are given in cm^{-1}. Element thicknesses t and all other dimensions given in cm. The ratio of the radius of the Petzval surface to the focal length is given by γ. This rather complex eyepiece is interesting because the Petzval curvature is so small. The tangential field is also well under control out as far as 36°. The Petzval curvature is kept small by using strongly curved surfaces as the outside surfaces of the lens. If this is done the glass used for the element nearest the field stop must be free of bubbles; otherwise they will be seen since they are so close to the focal plane. (From Military Standardization Handbook "Optical Design," MIL-HDBK-141, p. 14-18, 5 Oct. 1962.)

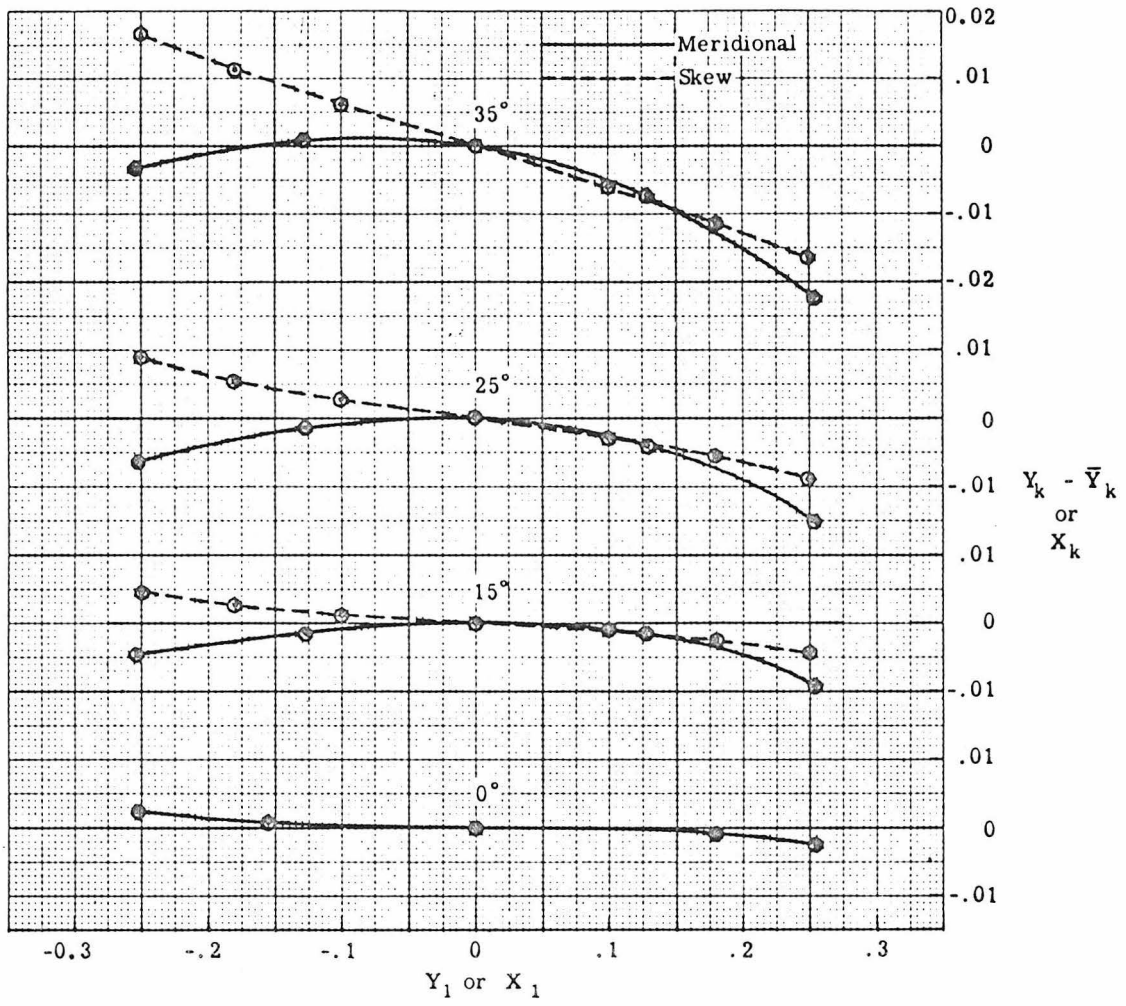

Fig. 11 Calculated meridional and skew fans for the Wild eyepiece of one inch focal length. Ray aberrations are given for various field angles. Meridional aberration $Y_k - \bar{Y}_k$ is given as function of coordinate of intersection Y_1 of ray with aperture, skew aberration X_k as function of intersection coordinate X_1. All dimensions are given in cm. Data are for rays entering left of lens through exit pupil from source at infinity. (From Military Standardization Handbook "Optical Design," MIL-HDBK-141, p. 14-19, 5 Oct. 1962.)

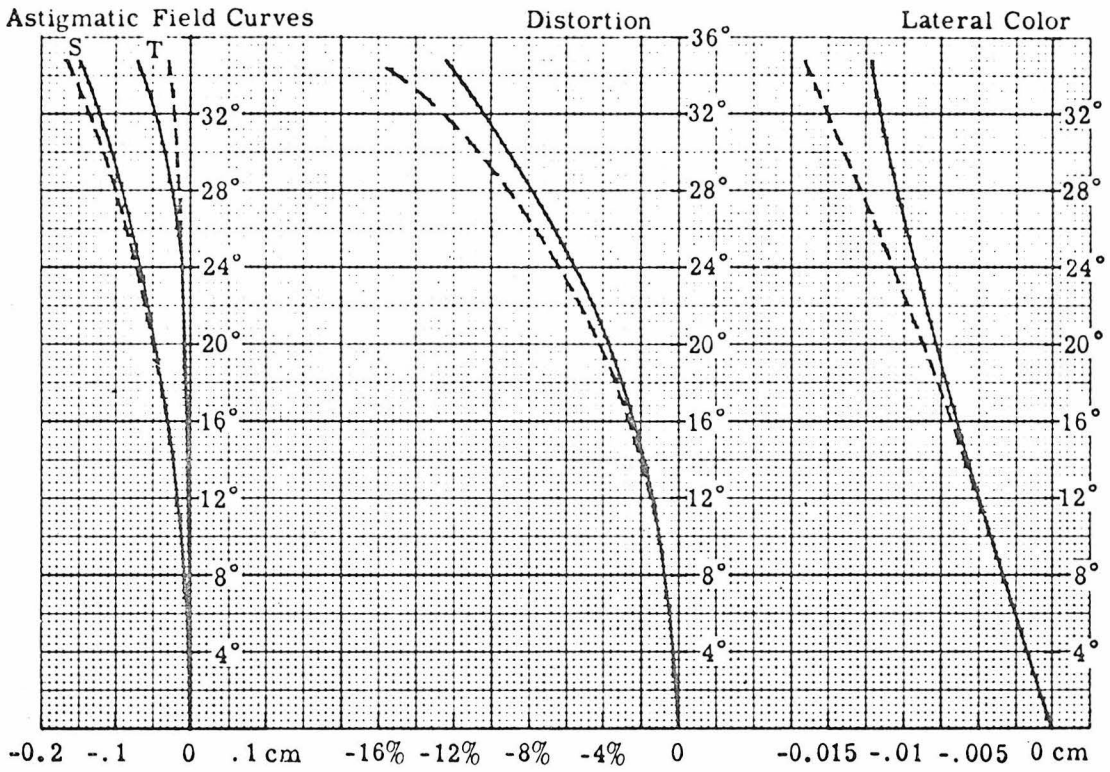

Fig. 12 Calculated sagittal (S) and tangential (T) fields, distortion, and lateral color curves for the Wild eyepiece of one inch focal length. Dashed curves are from third order analysis. (From Military Standardization Handbook "Optical Design," MIL-HDBK-141, p. 14-19, 5 Oct. 1962.)

$$\omega_{cW} = .18\,\psi^2 \text{ (N.A.)} \tag{40}$$

for the half angle of divergence ω_{cW} of the aberration cue associated with the worst ray of field curvature of the Wild eyepiece, where ψ is the half-field angle. These data pertain to objects located at infinity. However, we shall assume that they are also approximately valid for objects at finite, but reasonably large distances (say > 10 f).

The expression for blurring due to curvature and astigmatism for the Wild eyepiece is only very slightly smaller than that of the fly's eye lenslet (cf. table 1). This is somewhat misleading however. The fly's eye aberrations are derived from third order theory, and at large angles do not fully account for image degradation. Equation (40), though, is valid even for $\psi = 35^{\circ}$. Second, the expression $.22\,\psi^2$ (N.A.) given for the fly's eye aberration is based upon the least circle of confusion radius. In the fly's eye lens we may form the emulsion as an integral part of the lens and it is relatively easy to curve the emulsion surface to minimize the degradation due to field curvature. But we assume that the Wild eyepiece is used with flat film, which cannot lie in the curved least circle of confusion surface. On the other hand, coma and spherical aberration are negligible here. Most important though is the fact that we may use values of N.A. $< \psi$ and still get completely filled bundles of rays in the stereogram.

Distortion is considered in some detail in Appendix III. According to the results obtained there, we shall consider the effects of distortion to be negligible.

4.4 Choosing Parameters for the Holographic Stereogram Camera

The resolution of the fly's eye lens, as we have seen, is nearly always limited by aberrations. Furthermore, if we wish the ray cones to be completely filled, an optimized fly's eye lens obeys the relation (33), $\psi \cong$ N.A., and the aberration-limited angular resolution is therefore determined solely by the half-field angle ψ. The N.A. of the lens used for stereogram applications, however, is usually much smaller than ψ and may be varied. In particular, after determining from Section 3.3 the aperture size which balances the diffraction cue appropriately with the focus cue, we may then choose an eyepiece which is sufficiently largely scaled (i.e. with large enough focal length) to decrease the N.A. to the extent that aberrations are no worse than the blurring associated with these cues. We shall derive in this section the minimum focal length which must be used to accomplish this. If we use an eyepiece of too short focal length so that aberrations are significant, it is advantageous to decrease the aperture size, and hence aberrations, until the resulting diffraction effects become comparable. We shall investigate this case also, and find the degradation caused by a small eyepiece.

First consider a finite object, of height $\sim h$, depth $\sim L$, at a distance $\sim d$ from the camera aperture. For this case we wish to minimize the linear element of resolution ε. The approximate half-field angle ψ_L is given by

$$\psi_L \cong \frac{h}{2d} , \tag{41}$$

so that the half-angle of the aberration cue ω_{cL} is

$$\omega_{cL} \cong \beta \left(\frac{h}{2d}\right)^2 (\text{N.A.}) \tag{42}$$

for sufficiently small (N.A.), where β is a constant dependent upon the lens design. For the Wild eyepiece, $\beta = 0.09$. This value is one half of 0.18, the value given in (40) – it is assumed that the film is located closer to the lens than the Gaussian image plane by a distance equal to half of the axial distance occupied by the curved image surface, thus reducing the associated worst blurring by a factor of ~ 2. The amount of shift of the film depends, of course, upon the half-field angle which we choose. Setting (N.A.) = a/f, where a is the aperture radius and f the focal length, and solving for the value of f such that $\omega_{cL} = \omega_{oL}$, where $\omega_{oL} = (L\lambda)^{1/2}/2d$ is the resolution limit from (34), we find

$$f_{oL} = \frac{\beta h^2}{2L} \tag{43}$$

as the minimum focal length for which aberrations are negligible. We should also note that the numerical aperture for this value of f, $(\text{N.A.})_{oL}$, is given by (cf. (24))

$$(\text{N.A.})_{oL} = \frac{a}{f_{oL}} = \frac{\alpha d}{f_{oL}} = \frac{d}{f_{oL}} \left(\frac{\lambda}{L}\right)^{1/2} = \frac{2}{\beta} \left(\frac{d}{h}\right) \left(\frac{\lambda}{h}\right)^{1/2} \left(\frac{L}{h}\right)^{1/2} . \tag{44}$$

In practice, we must verify that $(\text{N.A.})_{oL}$ is sufficiently small ($\lesssim 0.1$ for the Wild eyepiece) so that (42) is valid. For example, for $\beta \sim 0.1$ and $h \sim L$,

$f_{oL} \sim \frac{h}{20}$, and if $\frac{d}{h} \sim 3$, $(N.A.)_{oL} \lesssim 0.1$ for $h \gtrsim 7''$. Therefore, the Wild eyepiece described in Figs. 10 – 12 performs almost perfectly for objects in the range $\lesssim 20''$. In the extreme close range our specification of the aberration blurring is not precise because of the finite conjugates; however, this effect is probably offset by the use of smaller N.A. here.

In the event that we must use an eyepiece of shorter focal length f, we balance the diffraction blurring ω_{diff} against the aberration blurring ω_c:

$$\omega_c = \omega_{diff} \tag{45}$$

or

$$\beta \left(\frac{h}{2d} \right)^2 (N.A.) = \frac{\lambda}{2f(N.A.)} \quad , \tag{46}$$

which yields

$$(N.A.) = \left(\frac{2d}{h}\right) \left(\frac{\lambda}{2f\beta} \right)^{1/2} = (N.A.)_{oL} \left(\frac{f_{oL}}{f}\right)^{1/2} \tag{47}$$

and

$$\omega_c = \omega_{diff} = \omega_{oL} \left(\frac{f_{oL}}{f}\right)^{1/2} \tag{48}$$

for

$$f \leq f_{oL} \quad .$$

Next consider a scene which extends from a distance d to infinity, of half-field angle ψ, so that the half angle $\omega_{c\infty}$ of the aberration cue is

$$\omega_{c\infty} = \beta \psi^2 \text{ (N.A.)} \tag{49}$$

for sufficiently small N.A.. Here we wish to optimize angular resolution. Solving for the value of f for which $\omega_{c\infty} = \omega_{o\infty}$, where $\omega_{o\infty} = \frac{1}{2} (\frac{\lambda}{d})^{\frac{1}{2}}$ is the resolution limit from (30), we obtain

$$f_{o\infty} = 2\psi^2 \beta d \tag{50}$$

as the minimum focal length for which aberrations are negligible. The N.A. for this value of f, $(\text{N.A.})_{o\infty}$, is given by (cf. (29))

$$(\text{N.A.})_{o\infty} = \frac{a}{f_{o\infty}} \quad \frac{(\lambda d)^{\frac{1}{2}}}{f_{o\infty}} = \frac{1}{2\psi^2\beta} (\frac{\lambda}{d})^{\frac{1}{2}} . \tag{51}$$

The N.A. must be sufficiently small in order that (49) be valid. For the one inch Wild eyepiece in particular, imaging is essentially aberrationless for scenes in which $d \lesssim 20''$, from (50).

If a focal length shorter than $f_{o\infty}$ is used, we balance diffraction against aberrations (cf. (46)):

$$\beta\psi^2 \text{ (N.A.)} = \frac{\lambda}{2f \text{ (N.A.)}} . \tag{52}$$

The solution of this is

$$\text{N.A.} = \frac{1}{\psi}\left(\frac{\lambda}{2\beta f}\right)^{1/2} = (\text{N.A.})_{o\infty}\left(\frac{f_{o\infty}}{f}\right)^{1/2} \tag{53}$$

and

$$\omega_c = \omega_{\text{diff}} = \psi\left(\frac{\beta\lambda}{2f}\right)^{1/2} = \omega_{o\infty}\left(\frac{f_{o\infty}}{f}\right)^{1/2} \tag{54}$$

for

$$f \leq f_{o\infty} .$$

4.5 Exact Form of the Holographic Stereogram Image

It is of interest to express the image in exact form, in terms of the object and lens characteristics. This is generally very difficult to do, but can be done if these characteristics are of very simple nature. In particular, we shall assume that the aberrations of the wavefronts caused by the lens system are negligible, so that we deal only with spherical wavefronts. As we have done previously, most of the discussion will center upon object rather than image space. Matters are simplified by this, since no propagation through glass occurs between the aperture and the object.

First, let us determine the conditions required in order that the wave aberration be negligible. We consider propagation of light from a point in image space to its conjugate point in object space, and we wish to determine the optical distance between the wavefront which intersects the center of the aperture, and the reference sphere centered on the conjugate point which also intersects

the center point of the aperture. We measure the distance normal to the wavefront, and assume that the object point is close to axis, so that a ray intersects the aperture plane, wavefront, and reference sphere at almost the same distance from the optical axis. We assume that the reference sphere and wavefront are nearly coincident – the wavefront aberration is thus the same even if we interchange the source and conjugate point.

It can be shown that to a good approximation the optical path difference or wave aberration $\Phi(\bar{\rho})$ associated with the aperture coordinate $\bar{\rho}$ is given by[15]

$$\Phi(\bar{\rho}) = \int_0^{\bar{\rho}} \frac{\bar{\Delta}(\bar{\rho}')}{R} \cdot d\bar{\rho}' , \tag{55}$$

where $\bar{\Delta}(\bar{\rho})$ is the transverse ray aberration associated with a ray from the point in image space passing through the aperture at the point $\bar{\rho}$ in a coordinate system in which $\bar{\rho} = 0$ is the center point of the aperture. R is the aperture to object distance, so that the angular aberration $\bar{\omega}_{ab}(\bar{\rho})$ is defined by

$$\bar{\omega}_{ab}(\bar{\rho}) \equiv \frac{\bar{\Delta}(\bar{\rho})}{R} . \tag{56}$$

For the paraxial case, $\bar{\Delta}(\bar{\rho})$ and $\bar{\omega}_{ab}(\bar{\rho})$ lie in a plane transverse to the optical axis. For field curvature alone, $\bar{\Delta}(\bar{\rho}) \parallel \bar{\rho}$[16]; the existence of some astigmatism and small residuals of other aberrations changes this slightly, but if in accordance with (42) and (49) we set

$$\bar{\omega}_{ab}(\bar{\rho}) = \beta \psi^2 (\text{N.A.}) \frac{\bar{\rho}}{|\bar{\rho}|} \quad , \tag{57}$$

we shall obtain an approximate upper limit for $\Phi(\bar{\rho})$. From (55), (56), and (57) we obtain

$$\Phi(|\bar{\rho}| = a) = \beta \psi^2 f \int_0^{(\text{N.A.})} (\text{N.A.})' \, d(\text{N.A.})' \tag{58}$$

$$= \beta \psi^2 f \frac{(\text{N.A.})^2}{2} \quad .$$

Suppose we wish to image a finite object and we set f and (N.A.) to the values (cf. (43) and (44)) necessary to reduce aberrations to the resolution limit. We then have for the maximum wavefront aberration

$$\Phi_{oLmax}(|\bar{\rho}| = a) = \frac{\lambda}{4} \quad . \tag{59}$$

The notation is analogous to that of (43) and (44). Similarly, using the values of f and (N.A.) given by (40) and (41) for a scene extending from d to infinity,

$$\Phi_{o\infty max}(|\bar{\rho}| = a) = \frac{\lambda}{4} \quad . \tag{60}$$

Therefore, in these cases, the Rayleigh criterion for a perfect wavefront is met. Of course, we may further increase f and proportionally decrease $\Phi(|\bar{\rho}| = a)$.

It may be recalled from Section 2.3 that the pinhole camera is best used in the range $u \sim \pi$ (cf. (8)). For the holographic stereogram, since

the depth of focus extends on both sides of the vertex of the focus cue, it can be shown that the depth of focus is given by $-2\pi \lesssim u \lesssim 2\pi$. By referring to Fig. 2 we find that the v-dependence of the intensity of the image of a point source is nearly independent of u for $|u| \lesssim \pi$. It can be shown that for this range of u, corresponding to approximately one half the depth of focus region for a finite object, setting $u = o$ yields a wavefront error of $\lambda/4$ at most in any contribution to the Kirchhoff integral.[17] For $u = o$, i.e. the Fraunhofer limit, the image of the point source is simply the Airy pattern. The treatment here will be limited to cases for which this approximation is valid. A generalization to arbitrary values of u is straightforward. The treatment is also limited to object points close to the optical axis (say $\psi \lesssim 10^{o}$). A generalization to extreme angles is straightforward – the aperture is then seen obliquely from the object point; for $u = o$ the Airy pattern merely assumes elliptical rather than circular symmetry.[18]

Subject to the conditions stated above, a point source in image space yields an Airy diffraction pattern in object space, of constant phase (except for negative values) over a spherical surface centered on the aperture center point. Thus aside from a phase factor dependent only upon the source position in image space we have a spatially invariant impulse response from the film plane to any (paraxial portion of) spherical surface, lying well within the depth of focus, which is centered upon the aperture center point. Thus the scalar Green's function is given by

$$G(\psi', \phi', \psi, \phi, R) = \frac{e^{ikR}}{R} \frac{J_1(\frac{\delta 2\pi a}{\lambda})}{(\frac{\delta 2\pi a}{\lambda})} e^{im(\psi')} M(\psi') , \qquad (61)$$

where

J_1 = the first order Bessel function

ψ = azimuthal angle, measured from optical axis, of observation point, in spherical coordinate system in object space with origin at aperture center point

ϕ = meridional angle of observation point in same coordinate system

ψ', ϕ' = are coordinates on the film plane such that a source at (ψ', ϕ') would be imaged at $(\psi = \psi', \phi = \phi')$ if all image degradations except distortion were absent

δ = azimuthal angle in object space of the observation point, measured in a spherical coordinate system also centered at the aperture center point, but in which $\delta = 0$ corresponds to $\psi = \psi'$, $\phi = \phi'$

R = distance from aperture center to measurement point

k = optical wave number.

The phase dependence upon the source position is given by $m(\psi')$, in which circular symmetry is assumed. The optical path length along a ray from (ψ', ϕ') on the film plane to the aperture center is equal to $m(\psi')/k$. A slight asymmetry of the optical system could result in a ϕ' dependence of m,

however. $M(\psi')$ is a slowly varying amplitude gradation which accounts for field variations of glass transmittance, obliquity factors, etc., and also contains other uninteresting constants.

Since only paraxial imaging is considered here, we may approximate the segment of the sphere of radius R as a plane, and transform to rectilinear angular coordinates $\theta_1 = x/z$ and $\theta_2 = y/z$:

$$G(\theta'_1, \theta'_2, \theta_1, \theta_2, R) = \frac{M(0)}{z_o} e^{i[kR(\theta_1, \theta_2) + m(\psi')]} \frac{J_1(\frac{\delta 2\pi a}{\lambda})}{(\frac{\delta 2\pi a}{\lambda})} , \qquad (62)$$

where x, y, and z are linear coordinates fixed in object space and we have replaced, where appropriate, $M(\psi')$ by its paraxial value, and R by the z coordinate z_o of the sphere segment apex measured from an origin in the aperture plane. The exact value of $R(\theta_1, \theta_2)$ must be retained in the exponential, however. We also have:

$$\delta^2 = (\theta_1 - \theta'_1)^2 + (\theta_2 - \theta'_2)^2 , \qquad (63)$$

where (θ'_1, θ'_2) is the image point corresponding to (θ_1, θ_2), in transformed image space coordinates. It is assumed that the Green's function (62) is symmetrical under the coordinate inversion $(\theta'_1, \theta'_2) \rightleftarrows (\theta_1, \theta_2)$. Suppose an approximately (no micron-like precision necessary) plane object is located in the paraxial region of the plane in question, and is incoherently illuminated to have brightness

$$B(\theta_1, \theta_2) = B(\frac{x}{z_o}, \frac{y}{z_o}) \quad . \tag{64}$$

Then if we expose the i^{th} component photograph, the resulting intensity on the film plane is given by the convolution:

$$I(\theta'_{1i}, \theta'_{2i}) = \{B * |t|^2\} (\theta'_{1i}, \theta'_{2i}) \quad , \tag{65}$$

where

$$t(\eta_1, \eta_2) = \frac{J_1[\frac{2\pi a}{\lambda}(\eta_1^2 + \eta_2^2)^{\frac{1}{2}}]}{[\frac{2\pi a}{\lambda}(\eta_1^2 + \eta_2^2)^{\frac{1}{2}}]} \quad , \tag{66}$$

and a factor which is independent of $(\theta'_{1i}, \theta'_{2i})$ has been dropped. The subscript i is used to explicitly remind us that the origin of the coordinate system $\theta'_{1i}, \theta'_{2i}$ lies at a different position with respect to the optical axis for each component photograph. The origin of $\theta'_{1i}, \theta'_{2i}$ is at the image of the point $(\theta_1 = 0, \theta_2 = 0, z = z_o)$ in the i^{th} component photograph. It is obvious from (65) and (66) that because of the spatial band-limited nature of t we cannot determine, or hope to reconstruct, the function B exactly without some a priori knowledge, e.g. that B is appropriately band-limited (cf. Section 6.6). This limitation obviously also applies when aberrations are present.

The film is processed to provide amplitude transmittance proportional to $I(\theta'_{1i}, \theta'_{2i})$, returned to position, and coherently illuminated as described in Section 4.2. If the illumination is by a plane wave normally incident on the film, the resulting amplitude in the plane $z = z_o$ is, neglecting uninteresting

constants,

$$A_i(\theta_1,\theta_2)\Big|_{z=z_o} = e^{ikR_i(\theta_1,\theta_2)} \{(\beta_i I) * t\}\ (\theta_1,\theta_2)$$

$$= e^{ikR_i(\theta_1,\theta_2)} \{[\beta_i(B * |t|^2)] * t\}(\theta_1,\theta_2)\ , \tag{67}$$

where

$$\beta_i(\theta'_{1i},\theta'_{2i}) = e^{im(\psi')}\ T_i \tag{68}$$

and $R_i(\theta_1,\theta_2)$ is the distance from the aperture center to the measurement point. T_i is a translation operation which transforms ψ' to the respective $(\theta'_{1i},\theta'_{2i})$ coordinate system.

The function β_i may be effectively reduced to unity by illuminating the processed film with a wavefront proportional to $e^{-im(\psi')}$. This is the purpose of the auxiliary lens of Fig. 8. From the ray path length interpretation of $m(\psi')$ in (61), we may also note that the auxiliary lens serves to focus the coherent illumination at the aperture center point when the transparency is not yet in place – with the transparency in place, the electric field in the aperture plane is proportional to the Fourier transform of the transparency amplitude transmittance for paraxial objects and images. Accordingly, we set:

$$\beta_i(\theta'_{1i}, \theta'_{2i}) = 1 \quad . \tag{69}$$

The amplitude $A_i(\theta_1, \theta_2)$ is recorded holographically, as described in Section 4.2 , and the operation is repeated for all aperture locations. Under holographic wavefront reconstruction, the electric field, measured in the plane where the object had been located, is the sum of contributions from each pinhole location:

$$A(\theta_1, \theta_2)\Big|_{z=z_o} = \sum_{i=1}^{n^2} A_i(\theta_1, \theta_2)\Big|_{z=z_o}$$

$$= \{B * |t|^2 * t\}(\theta_1, \theta_2) \sum_{i=1}^{n^2} e^{ikR_i(\theta_1, \theta_2)} \quad , \tag{70}$$

where n^2 is the number of (holographic) apertures contributing.

The function $e^{ikR_i(\theta_1, \theta_2)}$ fluctuates very rapidly with small changes in R_i and since no micron-like precision is maintained in positioning of the aperture, is a pseudo-random function. Therefore, for large n^2 the ensemble average intensity is given by

$$\langle |A(\theta_1, \theta_2)|^2_{z=z_o} \rangle = |\{B * |t|^2 * t\}(\theta_1, \theta_2)|^2 \tag{71}$$

where a constant proportional to n^2 is omitted. If we denote the spatial Fourier transforms of the respective functions by $a \sim$, and recall that t is real and circularly symmetrical, we have

$$\overbrace{\langle |A(\theta_1, \theta_2)|^2_{z=z_o} \rangle}\ (\bar{\omega}) =$$

$$\{\tilde{B}\tilde{t}(\tilde{t} * \tilde{t}) * \tilde{B}^*_- \tilde{t}\,(\tilde{t} * \tilde{t})\}\ (\bar{\omega}) \tag{72}$$

where

$$\tilde{B}^*_-(\bar{\omega}) \equiv \tilde{B}^*(-\bar{\omega}) = \tilde{B}(\bar{\omega})\ , \tag{73}$$

and $\bar{\omega}$ is the spatial frequency coordinate. The band width of this signal is equal to that of $|\tilde{t}|^2$. Thus, the system behaves much like an incoherent imaging system.

These results are considered further in Section 6.6.

CHAPTER FIVE

THE ACHROMATICALLY IMAGED FRESNEL ZONE PLATE

5.1 Introduction

The holographic stereogram is an array of minute holograms (refer to Figs. 8, 9). These component holograms can be made by nearly any of the well known procedures described in the holography literature. In particular, the discussion of Section 4.2 was based upon the use of the two-beam configuration of Leith and Upatnieks. In the holographic recording step, we are essentially making holograms of transparencies, and for this it is not necessary to have as highly coherent a source as that required for an extended object – this consideration has been studied in detail.[19 - 23] The general requirement for small path length differences between the object and reference beams is easily satisfied in our case because of the small portions of the holographic plate individually exposed.

An elegant way to minimize the path length differences when source coherency is limited is the achromatically imaged grating technique of Leith and Upatnieks[22] (hereinafter referred to as L&U) in which a diffraction grating acts as the beam splitter to divide the object and reference beams. Recently Kato and Suzuki[23] (hereinafter referred to as K&S) have used a configuration similar to that of L&U, but in which a zone plate is substituted for the diffraction grating in order to obtain Fourier transform, rather than Fresnel transform holograms.

As has been previously noted,[24] an adaptation of L&U's method can also be used for the holographic stereogram. An achromatically imaged zone plate is utilized, and Fourier transform holograms are produced. The arrangement is quite different from that of L&U or of K&S. The reduction in coherency requirements is not so great, however; partly because, as was noted above, the requirements here are not severe to begin with.

In addition to reducing coherency requirements, imaged gratings, or more generally imaged zone plates, provide a very neat method which could be utilized in many hologram arrangements for providing a reference beam. The discussion here is more physical than mathematical in emphasis, while no less rigorous than the previous treatments. The aim is to provide a method for visualizing by brief inspection the effects of source incoherence. It is hoped that this will be more useful for purposes of synthesis. The present method of analysis can easily be applied to the configurations of L&U and of K&S – the same results are obtained regarding coherency requirements.

The discussion is divided into two parts. In the first part it is shown that a two-beam holographic system in which the object beam is provided by the zeroth diffracted order of an achromatically imaged zone plate and the reference beam is provided by the first diffracted order has the same requirements for temporal and spatial coherence of the source as the same system used in the in-line mode, i.e. without the grating. Of course, the advantages of the two-beam process are retained; namely that the object transparency need not be nearly entirely transparent, and that in reconstruction the true image is separate from the illuminating beam and conjugate image. The analysis

could also be used to show that source coherency requirements are more severe if instead the first order diffracted wave is used as the object beam, as L&U have shown.

Having demonstrated the equivalence to operation in the in-line mode insofar as source requirements are concerned, the second part of the discussion is devoted to closer examination of the in-line mode of operation of the system. A method for visualization by inspection of the effects on image resolution of the source incoherency is described.

5.2 Application to the Holographic Stereogram System

The imaged zone plate configuration of the optical system used for the holographic stereogram is shown in Fig. 13. The purpose is to make a hologram in the aperture plane (plane e) of a transparency which is located a distance δ_a behind the back focal plane of the achromatic lens L_1. This arrangement is used to perform the second step of the holographic stereogram process, as described in Section 4.2 and as such is like Fig. 8, except that the coherent illumination is replaced by partially coherent illumination. Another difference is that the beam used to illuminate the transparency is not focused to a point in the aperture plane – therefore the general form of the function β_i ((68) rather than (69)) must be retained in the analysis of Section 4.5.

As shown in Fig. 13, the light from an incoherent source of pinhole dimensions is collimated by a lens L_S of focal length F_S. The light strikes an offset Fresnel zone plate in plane a, and the undiffracted light is used to

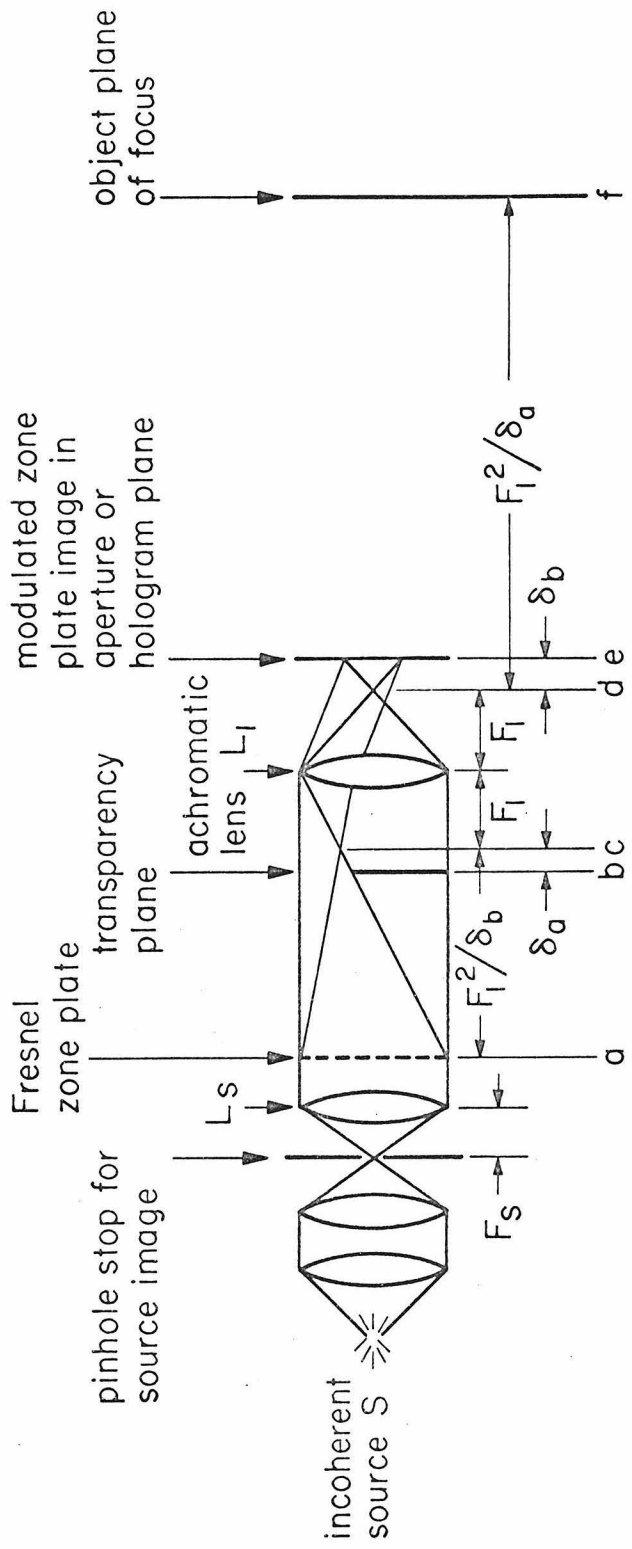

Fig. 13 Achromatically imaged Fresnel zone plate configuration of the holographic stereogram system, for step 2 of the process (cf. Fig. 8).

illuminate the transparency in plane b. The zone plate is designed to focus the first order wave to a point in the back focal plane of lens L_1, plane c.* This is transformed into a plane wave after propagation through the lens and is used as a reference beam for recording the hologram in plane e. The location of the transparency at a distance δ_a behind the back focal plane corresponds to a focus plane in object space at a distance F_1^2/δ_a from the front focal plane, from the Newtonian form of the image equation. For $\delta_a = 0$, Fourier transform holograms are produced and film resolution requirements are reduced. Similar advantages are gained in general for small values of δ_a. The zone plate has focal length F_1^2/δ_b,** where δ_b is the distance from the front focal plane d to the aperture plane e. The other first order diffracted wave from the zone plate is focused to a point midway between planes d and e and can be nullified by a small stop placed here if the object transparency is not in place, or otherwise by auxiliary components to the left of the transparency. If higher order waves are present, additional stops may be necessary.

If the object transparency is of uniform density, i.e. without any detail, the hologram is simply the interference pattern between the first order

---

*The light focused by the zone plate may pass through a clear portion of the transparency, in order to minimize path length differences.

**An elegant way to make the zone plate is by putting a photographic plate in plane a, and shining a plane wave at the desired angle back through lens L_1. If a left-traveling plane wave is provided at plane a, the exposed plate, when developed, is a holographic zone plate of the correct focal length.

wave and the attenuated but otherwise unperturbed zeroth order wave. This pattern is that of a Fresnel zone plate. In fact, we find from the Newtonian form of the image equation that plane e is the conjugate of plane a, so that this interference pattern is the image of the zone plate there. Therefore this pattern is independent of source coherency! Because of our use of stops and the attenuating transparency, this result is not quite trivial, but it is easily derived in Appendix IV.

5.3 Equivalence with Respect to Source Coherency Requirements of the Imaged Zone Plate to Gabor In-Line Holography

Referring again to Fig. 13, the in-line or Gabor holography mode of operation is as follows: the zone plate is removed from the system so that only the zeroth order wave is involved, and the transparency must be such that in the aperture plane e the AC portion of the field due to picture detail is much smaller in amplitude than the DC portion due to the average (usually high) transmittance of the transparency. The AC field is considered to interfere with the DC field and, as is well known, the relief of the reconstructed holographic image is reversed from that of the transparency. The image is degraded by the overlapping conjugate image.

5.3.1 Temporal Incoherence

The effect of temporal incoherence is studied by using a point source of approximate wavelength λ and spectral width $\Delta\lambda \ll \lambda$. We require that

the optical path length along a ray from the source to the transparency and from there along another ray to a point on the aperture plane differ by no more than $\lambda^2/4\pi\Delta\lambda$ from the optical path length of the appropriate reference beam with which it interferes. The reference beam associated with that point has traversed the same optical distance regardless of whether through the zeroth or first order beams, because of the imaging condition. And since the shape and – more important – the path lengths associated with the object wavefront are the same for a given picture for the in-line and imaged zone plate cases, we conclude that the two are equivalent with respect to temporal coherence requirements. Of course the imaged zone plate case is not restricted to low AC/DC ratios; this requirement is replaced by the need for low zeroth order to first order ratio which is satisfied by using a sufficiently dense transparency or by other means of attenuation.

We have implicitly assumed that it is sufficient to treat each portion of the transparency separately. This is valid because of the linearity of the holographic process; reconstructed field amplitudes are linearly related to the object fields.

5.3.2 Combined Spatial and Temporal Incoherence and the Modulated Zone Plate Image Concept

If the pinhole-sized source is self luminous, it exhibits spatial incoherence unless the pinhole is of infinitesimal dimensions. This phenomenon may be modeled by considering the source to be comprised of a number of mutually incoherent point sources uniformly distributed across the pinhole, each radiating

at the same wavelength. Each of the point sources in conjunction with a portion of the transparency produces an interference pattern in plane e; the sum of the intensities of the respective patterns is recorded as the hologram of this portion of the transparency. Of course the effects due to different parts of the transparency add linearly. However, the holographic patterns due to each of the respective point sources are displaced slightly from each other, and as a result the fine detail is blurred in the hologram.

While the details need not concern us here, it may be noted that the holographic pattern due to one of the point sources, together with an image point, is of the nature of a zone plate; and the fine detail thus corresponds to light diffracted far from the center of this pattern and therefore to transparency detail. In fact, temporal incoherence of the self-luminous source can be similarly treated. We can consider each point source to be comprised of a sum of monochromatic radiators of different wavelengths. The discussion of Section 5.3.1 is equivalent to this.

The important point is that each additive component of the hologram is the interference pattern between the appropriate object wave and either the zeroth order or first order diffracted beam of the imaged zone plate. Because of the imaging condition, however, the zeroth and first order beams differ by a phase factor, $\phi[\bar{r}(\bar{r}')]$ of Appendix IV, which is independent of the source and transparency. The true image components of the holographic patterns of the in-line and imaged zone plate cases therefore differ merely by a multiplicative factor $\phi[\bar{r}(\bar{r}')]$ which obviously carries no information (Q.E.D.). The imaged zone plate hologram may then be interpreted as a modulation of the function

$\phi[\bar{r}(\bar{r}')]$ by the in-line hologram pattern. Thus we have the concept of a modulated zone plate image, analogous to the modulated grating image concept of L&U.

5.4 Source Coherency Requirements for Imaged Zone Plate and Gabor In-Line Holograms

5.4.1 Temporal Incoherence Effects

According to the above discussion, we need only consider operation in the in-line mode. The method of inspection for temporal incoherence is by direct comparison of the optical path length of the zero order wave which can be measured from the point of convergence in the front focal plane d in Fig. 13, and that of the object wave which can be measured from a point on the transparency. For small path differences, the comparison is effected by measurement of the distance between the two associated spherical wavefronts. The wavefronts have a point in common where the ray connecting the transparency point with the convergence point intersects the hologram plane e.

5.4.1.1 A Method for Quick Inspection

The method is illustrated in Fig. 14. The zero order wavefront is centered upon the convergence point, and has radius of curvature $\sim \delta_b$. The object wavefront has radius of curvature s, where s is the distance from the hologram to the plane of focus in object space. Based upon the maximum path length difference $\lambda^2/4\pi\Delta\lambda$, the effective aperture radius a_t is

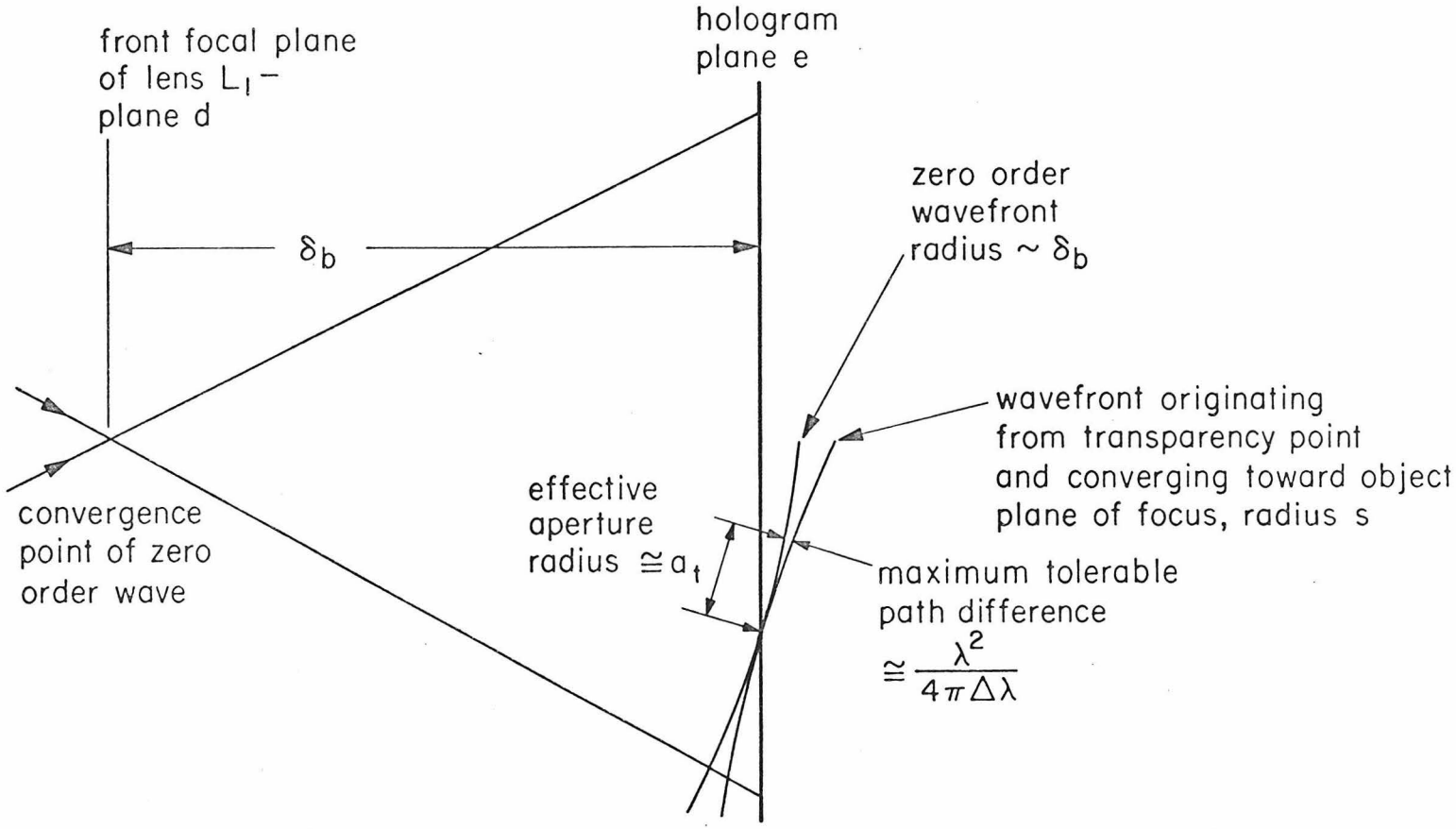

Fig. 14 A method for quick inspection of the effect of source temporal incoherence $\Delta\lambda$ on the resolution of an achromatically imaged Fresnel zone plate or Gabor in-line hologram. The temporal-incoherence-limited angular resolution ω_t is given by $\lambda/2a_t$, where the effective aperture radius a_t is $a_t \cong \lambda[s\,\delta_b/2\pi\Delta\lambda\,(s+\delta_b)]^{1/2}$, for δ_b and s the respective radii of curvature of the zeroth order diffracted wave and of the wave originating from a point on the transparency. (Opposite senses of curvature are assumed for the two wavefronts – cf. Fig. 13.)

$$a_t \cong \lambda \left[\frac{s\,\delta_b}{2\pi\Delta\lambda(s + \delta_b)} \right]^{1/2} \tag{74}$$

and the associated angular blur ω_t in the hologram reconstruction is given by (from an analogous diffraction problem)

$$\omega_t = \frac{\lambda}{2a_t} \cong \left[\frac{\pi\Delta\lambda(s + \delta_b)}{s\,\delta_b} \right]^{1/2} , \tag{75}$$

and since $s >> \delta_b$,

$$\omega_t \cong \left(\frac{\pi\Delta\lambda}{\delta_b} \right)^{1/2} . \tag{76}$$

5.4.2 The Effects of Finite Source Size

As was noted in Section 5.3.2, the restriction on source size is determined by the condition that the detail in the hologram must not be destroyed by what was envisioned there as a superposing of the differently displaced interference patterns of the point source components of the finite source.

The center of the pattern due to each conceptual point source and an image point on the transparency lies on the ray connecting these points, and therefore a translation of the image point will also effect a displacement of the pattern. The relative effects of source and image point displacements

are found by noting what image point displacement is required to counteract the effect of a source movement so that the ray connecting the two does not move on the hologram plane. A ray projection, through a point on the hologram, of the (circular) source pinhole onto the transparency plane is a disc, and the effect of the finite pinhole is therefore identical to convolution of the image with a disc of this diameter. The effect of the finite pinhole is not severely degrading if the smallest picture element is of linear dimension equal to the radius of the disc.

5.4.2.1 A Simple Mnemonic

The ray projection construction described above is most easily performed with respect to an image of the source pinhole, if such an image lies closer to the hologram plane than the pinhole itself. In the holographic stereogram application, such an image lies in the front focal plane d. The construction is illustrated in Fig. 15. The source image is of radius r_S' and the angular blur ω_s, caused by spatial incoherence for a self-luminous source is given by

$$\omega_s = \frac{r_S'}{\delta_b} \quad . \tag{77}$$

The similarity of this construction to that of the focus cue should be noted as a mnemonic. However, the physical basis of the construction is entirely

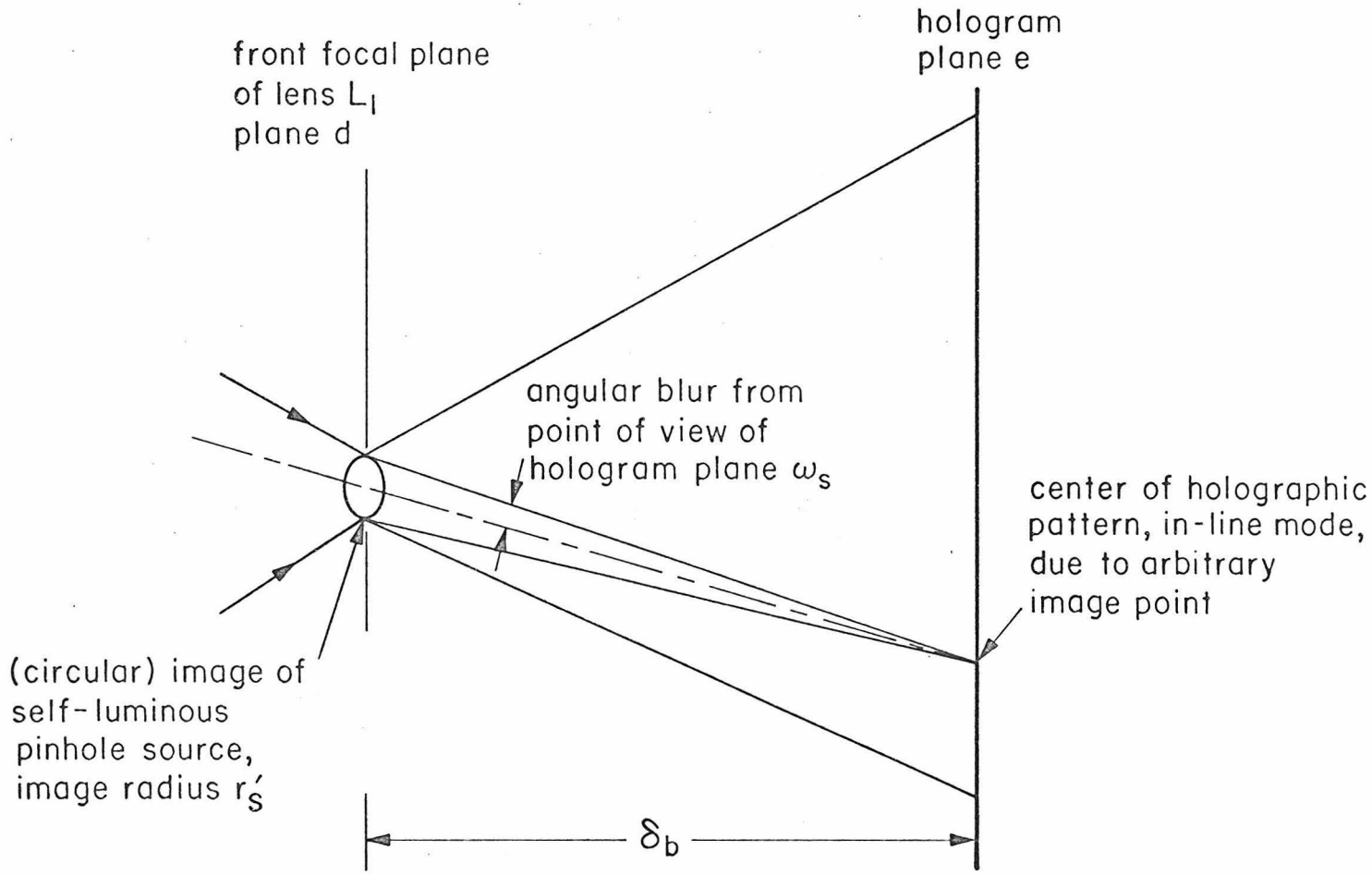

Fig. 15 A simple mnemonic for determining the effect of a self-luminous source of finite dimensions on the resolution of an achromatically imaged Fresnel zone plate or Gabor in-line hologram. The angular blur ω_s from the point of view of the hologram, due to source size, is equal to the angle subtended by the source image radius. (cf. Fig. 13.)

different from that of the focus cue. In particular, making r_S' infinitesimal does not cause diffraction blurring of the image.

We may define an effective aperture radius a_s

$$a_s \equiv \frac{\lambda}{2\,\omega_s} \quad . \tag{78}$$

5.5 An Example

Suppose we wish to use a white light source of brightness B in conjunction with an optical bandpass filter of width $\Delta\lambda$ and approximate wavelength λ to form a hologram. The image of the filtered source has brightness $\sim (\frac{\Delta\lambda}{\lambda})B$, neglecting transmission losses. The intensity I of the reference beam on the hologram surface is therefore given by

$$I \cong \pi (\frac{\Delta\lambda}{\lambda} B)\omega_s^2 \cong B \frac{\overset{\delta}{b}}{\lambda} \omega_t^2 \omega_s^2 \quad . \tag{79}$$

We would normally arrange to have $\omega_t = \omega_s$, and the total blurring effect would be approximated by

$$\omega \cong (\omega_t^2 + \omega_s^2)^{\frac{1}{2}} \quad , \tag{80}$$

so that

$$I \simeq \frac{B}{4} \left(\frac{b}{\lambda}\right)^{\delta} \omega^4 \quad . \tag{81}$$

Since $\omega_t = \omega_s$, we have $a_s = a_t$. Because contributions on a given hologram from different transparency points are not coincident, some overlap of adjacent holograms may be useful for providing completely filled out cones of rays in the stereogram image. The overlap factor N is, using (75), (76), and (80),

$$N \simeq \frac{\psi \delta}{a_t} \left(\frac{b}{\lambda}\right) \simeq \frac{2^{1/2} \psi \omega \delta}{\lambda} b \quad , \tag{82}$$

and we have used the fact that the zero order wave convergence half angle is $\sim \psi$.

CHAPTER SIX

OTHER FEATURES OF THE HOLOGRAPHIC STEREOGRAM

6.1 Introduction

We have seen that the fly's eye lens stereogram represents a marked advantage over the pinhole camera stereogram. We have also noted some important differences between the fly's eye lens and the holographic stereogram. These include:

Speed. An important advantage of the fly's eye lens hologram over the holographic stereogram is that it is a much quicker process. The holographic stereogram process is sequential in nature. A bank of cameras could be used to take the component photographs, but even then the process would be slower than the fly's eye lens by a factor of $[\psi/(\text{N.A.})]^2$, where ψ is the half-field angle and N.A. is the numerical aperture used in the camera. However, the condition $\psi > \text{N.A.}$ is chosen solely for the purpose of reducing aberrations, so that the slower process yields a better resolved image. For given designs of the fly's eye lenslet and of the holographic stereogram lens, one would in general have to decide to what degree resolution should be increased at the expense of time – completely aberrationless operation may be impractical.

Aberrations. This advantage of the holographic stereogram has been well noted. It should also be noted here that a disturbing effect of fly's eye lens images is the appearance of an anomalous image at angles $\psi > \Psi = \text{N.A.}$, where N.A. is the numerical aperture of the fly's eye lenslet. Typically, the image appears to jump about when one varies his position for viewing. This

effect can be eliminated by the use of baffles between adjacent lenslets which however adds complexity to manufacture of the lens.

Tunnel effect. This effect is actually a disadvantage of Pole's direct application of holography to fly's eye lens stereoscopy. It can be overcome if reflection rather than transmission holograms are made by Pole's method.

There are several other features of the holographic stereogram and ways for using it which deserve special mention. Each of these features represents an advantage of the holographic stereogram over the classical hologram, the fly's eye lens stereogram, or both.

6.2 Practical Advantages of the Process

The holographic stereogram is in many ways easier to make than the fly's eye lens stereogram. In the first place, it is quicker to obtain a single lens of arbitrary design than to tool up for production of a special fly's eye lens. Conventional components can be used for imaging and for such auxiliary purposes as illumination, making the design much more flexible; a good example of this is the achromatically imaged zone plate. In fact almost any photographic lens may be used, even with a between-the-lens aperture. However, if the aperture stop is not in the hologram plane, some overlapping of adjacent component holograms may be necessary in order to assure completely filled out ray cones in the reconstruction. This effect was noted in connection with the imaged zone plate, and there are associated problems of increased film noise.[25] Obviously, greater precision is possible with the holographic stereogram, both in lens fabrication and film registration. Furthermore, arbitrarily fine resolution can

be achieved with any type of film by using sufficiently large component images. It is inevitable that some portions near the edges of the fly's eye lenslets are inactive in imaging. This problem can also be overcome with the holographic stereogram; by close fitting or overlapping of adjacent component holograms the associated screen effect can be reduced.

6.3 The Full-Color Stereogram

The holographic stereogram is basically an array of simple holograms, and most of the well known holographic techniques may be applied to these holograms. In particular, they may be made as full-color holograms. Problems exist in color holography, but good full-color reconstructions are possible if the reference beams associated with the primary colors are introduced from different angles, or if thick holographic material is used. A distinct advantage over the use of color film in, say, a fly's eye stereogram, is the greater color saturation due to the use of spectral lines. An alternative approach which by-passes the problems of color holography and is well suited to stereograms is spatial color multiplexing. Each component photograph is taken through a filter of an appropriate primary color, and filters are incorporated into the component holograms for viewing. In a hexagonal close packed lattice of holograms, for example, there are three different and equivalent lattices, each one of which could be used for one primary color. The color saturation advantage is retained if narrow-band-pass filters are used with any of a variety of possible illumination sources. Spatial multiplexing can also be used with classical holograms. It should also be noted that component holograms of the holographic stereogram

can easily be made at a variety of wavelengths; by use of the achromatically imaged zone plate, a partially coherent source other than a laser may be used.

6.4 Distortionless Scaling

The operation of distortionless scaling is applicable to the holographic stereogram but not, to the author's knowledge, to either fly's eye lens stereograms or classical holograms. This subject is treated in detail in Appendix V.

6.5 The Focused-Type Holographic Stereogram

One difficulty with a typical hologram of a small object is that the viewer must move close to the hologram and look through it, as through a small window. The image typically appears somewhat behind this window, and if the viewer moves back he cannot see the image unless its apparent position is in his line of sight with the hologram. Also, incoherency in the illuminating source yields an apparent angular blur from the point of view of the hologram plane, and hence considerable linear blur may appear if the image location is far from the hologram plane. A solution to both problems is to make the hologram so that the image is approximately in coincidence with the hologram plane, and this is called a focused-type hologram.

The author is not aware of any method for directly making a focused hologram in which the image extends front and back of the hologram plane. To do so would seem to require placing the object and hologram plate

simultaneously in the same location.* Even making a focused hologram in which the image is partly in contact with the hologram plane but not extending through seems precluded by the apparent impossibility of providing a reference beam, for a transmission hologram. An obvious way to obtain a focused hologram is to "take" a second hologram of the perfect real image of an unfocused hologram. In addition to image degradation, however, this approach leads to a "tunnel" effect – no image is seen unless the viewer's line of sight intersects both the (second) hologram and the virtual (first) hologram. Somewhat similar problems arise if we try to make a focused-type stereogram with a fly's eye lens.

In making a holographic stereogram, the object is not present to block the reference beam in the holographic step. As a result, reflection and transmission-type stereograms with the object partly in contact with the hologram plane are easily made. Some problems exist for illumination, but these are overcome in practice by using an eyepiece camera shaped like a cone with the aperture at the point around which illumination is easily provided.

The illumination problem can be overcome in another way which moreover permits direct synthesis of stereograms with the image extending through the stereogram plane. The camera aperture is imaged into object space, so that no physical aperture is present as an obstruction. Two identical lenses without spherical aberration are used, being placed symmetrically with their front

---

*Distorted (i.e. non-perfect) imagery can be accomplished by projecting a real image of the object onto the hologram plate. We are considering, throughout this work, only perfect or almost-perfect imagery, (cf. Section 1.2).

focal planes in coincidence, and the camera aperture placed at the back focal point of one. The aperture is imaged to the back focal point of the other lens, and there is somewhat less than one focal length of space available for the object beyond the (imaged) aperture plane. While lenses of sufficient focal length may not be available, a pair of parabolic mirrors may also be used; in this case the camera axis is offset from that of the mirrors and some tilting of the film plane may be used to compensate for field curvature in the mirrors.

6.6 Spatial Filtering of Holographic Stereogram Images

Because the response of the holographic stereogram can be spatially invariant, spatial filtering methods are easily applied, and the possibilities are unlimited.[26 - 28] Let us treat a simple example, based on the discussion of Section 4.5. We do not consider noise here.

Suppose the brightness pattern B we wish to record is band-limited to spatial frequencies ω such that $|\omega| < \omega_o$. We then choose the aperture size a so that $\tilde{t}$, the Fourier transform of t, is (dropping an uninteresting normalization constant)

$$\tilde{t} = 1 , \qquad |\bar{\omega}| \leq \frac{\omega_o}{2} ,$$

$$= 0 , \qquad |\bar{\omega}| > \frac{\omega_o}{2} , \tag{83}$$

i.e.,

$$a = \frac{\omega_o \lambda z_o}{2\pi} \quad . \tag{84}$$

The Fourier transform of the recorded intensity is (cf. (65))

$$\tilde{I} = \tilde{B}(\tilde{t} * \tilde{t}) \quad , \tag{85}$$

of bandwidth ω_o (i.e. $|\bar{\omega}| < \omega_o$) .

Suppose the film is reversal developed with appropriate gamma to obtain amplitude transmittance I. The resulting signal is processed in a holographic, or complex spatial filter of spectral response $1/(\tilde{t} * \tilde{t})$ and the signal B is obtained:*

$$\tilde{B}(\tilde{t} * \tilde{t}) \rightarrow \frac{1}{\tilde{t} * \tilde{t}} \rightarrow \tilde{B} \quad . \tag{86}$$

The signal B is again reversal developed with appropriate gamma to obtain $\sqrt{B}$. Since $\sqrt{\tilde{B}}$ and $\tilde{t}$ have bandwidth $\omega_o/2$, the use of the image $\sqrt{B}$ to project the holographic stereogram yields (cf. (71)) the ensemble average intensity:

---

*This filter's response is infinite for $\omega = \omega_o$. In practice, this problem is overcome by using a system in which the value of ω_o is slightly larger than the band limit of B, so that the filter $1/(\tilde{t} * \tilde{t})$ need not be accurate all the way to ω_o .

$$\langle \, |A|^2_{z=z_o} \, \rangle = |\surd B * t|^2 = |\surd B|^2 = B \, . \qquad (87)$$

Thus, if B is band-limited, the system can be made to image perfectly.

CHAPTER SEVEN

CONCLUSIONS

The techniques of holography have been found to provide an elegant means for obtaining highly resolved and perfect three-dimensional images of a large class of objects. However, due to limitations imposed by laser technology and the need for objects to maintain micron-like stability during exposures, classical holograms cannot always be made, particularly in the imagery of very large objects. To fill such needs and also to provide a less expensive method for imaging objects for which holography is possible, a study was undertaken of the holographic stereogram, a method for obtaining less highly resolved but otherwise perfect three-dimensional images. As the name implies, the process is partly holographic in nature, but it provides images of naturally illuminated objects. The holographic stereogram is also readily applied to computer generation of 3–D images, since the component photographs could be artificially synthesized.

Besides these anticipated results, several further advantages over the classical hologram were discovered. Readily available partially coherent sources can be used to make full-color stereograms, most notably in connection with spatial multiplexing and/or the achromatically imaged Fresnel zone plate. In contrast to holograms, holographic stereograms of the focused type may be made which do not display the tunnel effect and hence are conveniently viewed from a distance. Finally, distortionless scaling of the image is possible.

The concepts of diffraction cues and geometrical or focus cues were developed for the analysis of stereograms, and were found to be quite useful for general photographic purposes. A graphical mnemonic was devised which greatly simplifies all depth of focus considerations and an example was treated which clarifies the concept of hyperfocal distance.

The pinhole camera stereogram, historically the first attempted method for almost-perfect* stereogram imagery, was studied from a ray reconstruction point of view. As with all stereogram systems, objects were found to possess an inherent depth of focus L, given by

$$L \cong 2\epsilon^2/\lambda \quad , \tag{11}$$

where ϵ is the linear resolution element desired and λ is the wavelength of light. Image reconstruction with the pinhole camera stereogram requires that the pinhole camera array be placed within the available depth of focus of the object, and the number n of rays contributing to a real image is given by the inverse of the utilized fraction of the available depth of focus. The filling ratio of the cone of rays contributing to the real image is given by 1/N, where N is the number of resolvable lines in the virtual image, which is limited by the relation

$$N \leq 2\epsilon/\lambda \quad . \tag{18}$$

---

*Perfect except for resolution limitations.

The relation

$$n\left(\frac{N}{2\psi}\right)\left(\frac{\lambda}{\epsilon}\right) = 2 \qquad (21)$$

shows the mutual interaction between n, the number of rays contributing to a real image point; $(N/2\psi)$, the "sharpness" of the virtual image; and (λ/ϵ), the relative resolution.

The fly's eye lens stereogram of Lippmann, which also predates the holographic stereogram, was studied and found to have several important advantages over the pinhole stereogram. The ray cones are nearly completely filled out, and the fly's eye lens is optimally placed outside the depth of focus of the scene, so that the entire depth may be utilized. However, the fly's eye lens was found to be subject to aberrations which in typical cases reduce resolution by one or two orders of magnitude. For a finite object the degrading factor (ω_a/ω_{oL}) is given by

$$\frac{\omega_a}{\omega_{oL}} \simeq .04\left(\frac{h}{d}\right)^2\left(\frac{h}{L}\right)^{1/2}\left(\frac{h}{\lambda}\right)^{1/2} \qquad (36)$$

for $\omega_a > \omega_{oL}$, where h is the object dimension transverse to the optical axis, L the dimension parallel to the optical axis, d the lens to object distance, ω_a the angular blur due to aberrations, and ω_{oL} the best possible angular resolution in the absence of aberrations. In the case of a scene extending to infinity, the degrading factor is given by

$$\frac{\omega_a}{\omega_{o\infty}} \cong .04\ (2\psi)^3\ (\frac{d}{\lambda})^{\frac{1}{2}} \tag{38}$$

where ψ is the half-field angle. The fly's eye lens is therefore limited to small field angles.

The holographic stereogram has been shown to exhibit the same advantages over the pinhole stereogram as the fly's eye lens and the associated camera system can be scaled to eliminate aberrations for even extreme field angles. The Wild eyepiece camera was specifically treated, and the necessary focal lengths f_{oL} and $f_{o\infty}$ to eliminate aberrations for finite and infinite scenes respectively are

$$f_{oL} = \frac{\beta h^2}{2L} \tag{43}$$

$$f_{o\infty} = 2\beta\psi^2 d \tag{50}$$

where $\beta \cong 0.1$. If a shorter focal length f must be used, the respective degrading factors are

$$\frac{\omega_c}{\omega_o} = (\frac{f_{oL}}{f})^{\frac{1}{2}}\ ,\ (\frac{f_{o\infty}}{f})^{\frac{1}{2}} \qquad \text{(from (48), (54))}$$

$$\text{for} \quad \omega_c > \omega_o$$

where ω_c is the aberration-limited angular resolution. The exact form of the aberration-free image was derived for a relatively flat object. This form is interesting in itself, but it was further shown that by optical spatial filtering the stereogram can be made to behave like a low-pass system of the same bandwidth as for incoherent imaging, but in which the response is unity up to the spatial cutoff frequency. (The object intensity function must be band-limited for this result.)

Other notable features were found to set the holographic stereogram apart from the fly's eye lens. Such matters as scaling, the focused-type stereogram, and spatial filtering were noted above. The image jumping effect is absent and the screen effect can be eliminated. The choice of optical components and film is, of course, more flexible, and there is no great problem of precision. The tunnel effect is not present as it sometimes is in Pole's application of holography to the fly's eye lens. Also, the methods utilizing partially coherent light are not directly applicable with Pole's method.

The problem was considered of replacing a high quality photographic lens by a fly's eye array of $m \times m$ lenslets of equal total area, or by the holographic stereogram equivalent. This reduces the transverse resolution by a factor of m, and increases the depth of focus by m^2 – each of the resulting m elements of depth is m times as deep as the initial depth of focus.

Finally, the achromatically imaged Fresnel zone plate was treated. This is a technique of very general applicability in holography which compensates for source incoherency. A specific example of a holographic stereogram camera was treated. But the most important result was the development of two simple

graphical mnemonics for rapid analytical inspection of the effects of, respectively, temporal and spatial incoherence of the source in any achromatically imaged zone plate or Gabor in-line type holographic system. The author believes that these mnemonics will be very useful for purposes of synthesis.

Several simplifications were introduced into the analyses, and the results obtained are therefore in many cases not exact – this has been indicated by the use of approximate equalities where applicable. The results are precise only for paraxial objects and images, both because of our use of small argument approximations for trigonometric functions, and because of the use of scalar electromagnetic theory. For extreme angles (half-field angle $\psi \sim 35^{\circ}$) the results are probably inaccurate by $\sim 15\%$. In addition, as was noted, diffraction focusing was not accounted for in the parameter optimizations, for the sake of clarity in the presentation. The phenomenon was briefly described; in extreme cases, practical utilization of diffraction focusing could effect as much as a 25% increase in resolution, but usually only about half this much. The specification of the radii of the blur discs associated with aberrations was somewhat arbitrary. Finally, quasi-monochromatic illumination was generally assumed, and if broad-band illumination is used the formulas must be appropriately integrated over the spectrum.

APPENDIX I

ABERRATIONS OF THE FLY'S EYE LENSLET

The radii of the blur circles associated with each of the aberrations are[29]

$$\begin{aligned} &\text{spherical} - B\rho^3 \\ &\text{coma}^* - F\psi\rho^2 \\ &\text{astigmatism}^{**} - C\psi^2\rho \end{aligned} \qquad \text{(I–1)}$$

where ρ = radius of entrance pupil

ψ = field angle in radians, measured from axis in object space.

B, F, C are the respective aberration coefficients, given by[30] (for a spherical lens):

$$\begin{aligned} B &= \tfrac{1}{2}h^4K^2\left(\frac{1}{ns'} - \frac{1}{s}\right) \\ F &= \tfrac{1}{2}h^2K(1 + kh^2K)\left(\frac{1}{ns'} - \frac{1}{s}\right) \\ C &= \tfrac{1}{2}(1 + h^2kK)^2\left(\frac{1}{ns'} - \frac{1}{s}\right) \end{aligned} \qquad \text{(I–2)}$$

---

*radius of circle contributed by outermost zone of lens

**radius of circle of least confusion (geometrical), which equals ¼ length of astigmatic line.

where $-s$, s' are the object, image distances from the lens surface, n is the index of refraction, and K is the Abbe invariant given by

$$K = n\left[\frac{1}{r} - \frac{1}{s'}\right] \tag{I-3}$$

where r is the radius of curvature of the lens. When the entrance pupil coincides with the lens surface, the parameters k and h are given by

$$k = 0 \tag{I-4}$$

$$h = -1 . \tag{I-5}$$

Using the symbol $\gamma = -s'/s$, we have

$$K = n\left[\frac{n+\gamma}{(n-1)s'} - \frac{1}{s'}\right]$$

$$= \frac{n\,(1+\gamma)}{(n-1)\,s'} \tag{I-6}$$

and the respective aberration radii are given by

$$\text{spherical} \quad - \quad \left[\frac{n}{2(n-1)^2 s'^3}\right] (1+\gamma)^2 (1+\gamma n)\ \rho^3$$

$$\text{coma} \quad - \quad \left[\frac{1}{2(n-1)s'^2}\right] (1+\gamma)(1+\gamma n)\ \psi\ \rho^2 \tag{I-7}$$

$$\text{astigmatism} \quad - \quad \left[\frac{1}{2ns'}\right] (1+\gamma n)\ \psi^2\ \rho .$$

Finally, to obtain the expressions in Table 1, we substitute N.A. = $\rho n/s'$, and $\psi = \psi$, the half-field angle.

APPENDIX II

Reprinted from

Volume 12, Number 1 **APPLIED PHYSICS LETTERS** **1 January 1968**

HOLOGRAPHIC STEREOGRAM FROM SEQUENTIAL COMPONENT PHOTOGRAPHS*

J. T. McCrickerd and Nicholas George
California Institute of Technology
Pasadena, California 91109
(Received 5 September 1967; in final form 27 October 1967)

Holograms of naturally illuminated objects are synthesized in two steps. A stereoscopic camera technique is used to record the objects' parallax qualities in white light; this photographic information is transformed into a hologram with coherent light. The image quality is excellent, and the method seems practical for making full-color reconstructions using stereoscopic photographs taken with color film.

A two-step method is described for holographically recording 3-D images of incoherently illuminated objects. R. V. Pole has previously demonstrated another method for this, using a "fly's eye" lens.[1] Both methods are applications of holography to stereoscopic photography,[2-3] particularly of the type proposed by Lippmann.[4] In the techniques described below, an ordinary camera lens is used to record the component photographs in sequence, rather than simultaneously as in the "fly's eye" lens case. This has two important consequences. First, the component photographs can be made much larger, and any kind of film can be used without loss of resolution. Second, the prior problem of screen effect caused by dead space between adjacent lenses of the "fly's eye" is eliminated.

The method involves two steps. In the first step, a sequence of ordinary photographs is taken of the incoherently illuminated object, providing a stereoscopic record. Each photograph is taken from a different segment of a reference plane. In the second step, a Fourier transform hologram of each photograph is recorded on the corresponding segment of a hologram plate which is placed in the reference plane. This requires a laser and other appropriate holographic equipment.

Figure 1 illustrates the taking of a typical photograph from a segment of the observation plane, $z = z_{ob}$; a mask is placed in this plane with a pinhole aperture centered at P_a. Behind the mask and aligned with the aperture are placed a convex lens and a sheet of photographic film. The lens-film system is focused to record the image, at P_i, of the object point P_0. For convenience the aperture diaphragm has been placed in front of the lens in order to be physically accessible as a light mask in step 2.

The resolution of the picture is affected by the aperture size, which is chosen small enough to provide adequate depth of focus, but not of wavelength dimensions, so that diffraction effects due to this aperture are minimal.

If the film is processed and returned to the original position, illumination of the image point P_i will cause a light ray to propagate through the small aperture to the object point P_0. We may, as shown in Fig. 2, interrupt this ray with a high-resolution photographic plate, immediately to the left of the aperture. When the image point is coherently illuminated, and the aperture additionally illuminated with a coherent reference beam, at an angle θ, the ray is holographically recorded at the point P_a of the high resolution plate. The object is not present in this step.

If one were to view this hologram, the normal illumination for the two-beam configuration of Leith and Upatnieks is used,[5] i.e., a coherent plane wave is beamed onto the plate, at angle θ, as shown in Fig. 3; the reconstructed ray emanates from P_a to the point P_0. The sensitivity of the reconstruction with θ is small, as described in the literature.[4]

The entire process may be repeated at point P'_a on the high-resolution plate, after translating

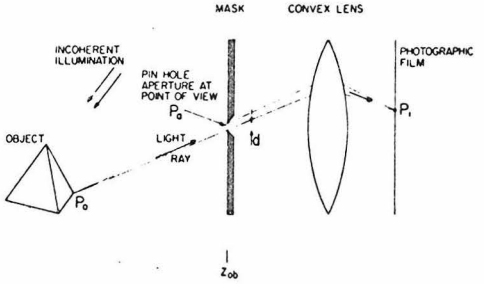

Fig. 1. Taking a typical photograph through pinhole aperture in the plane $z = z_{ob}$. (Lens-film-pinhole system shown in exaggerated scale.)

*Research supported in part by the Electronics Division of the Air Force Office of Scientific Research.

Volume 12, Number 1 APPLIED PHYSICS LETTERS 1 January 1968

pinhole, lens, and all, to align the system along P'_n. Fresh film is used to take the corresponding photograph. As shown in Fig. 3, the coherent plane wave illumination will then also result in a ray propagating toward P_0 from the point P'_n on the plate.

The process is repeated for all points of a two-dimensional lattice on the high-resolution plate. When the developed plate is plane wave illuminated, the many rays converging at the point P_0 will form an observable pseudoscopic real image there, of the object point. All object points are reconstructed this way. If we illuminate the developed plate from the opposite direction, the desired orthoscopic virtual image is observed.

Several holograms have been made by this method. The sequence of photographs is taken with a 16 mm motion picture camera, with a 0.05″ pinhole aperture mounted in front of its Switar 25 mm lens. The camera is mounted on a two-dimensional translator to facilitate movement to sequential points of view, which are spaced 0.05″ apart; and, of course, all of the step 1 photographs are taken in sequence, and then the step 2 holograms are made. Adequate registry is obtained with the unmodified film transport mechanism of the 16 mm camera. Kodak Plus-X reversal film is used.

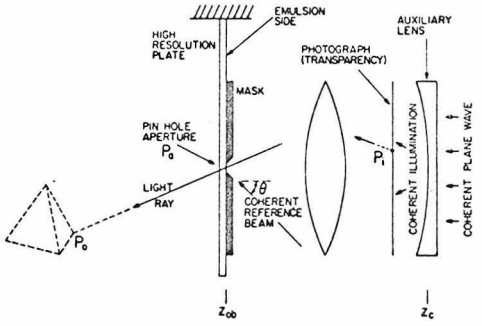

Fig. 2. Synthesis of hologram on high-resolution photographic plate.

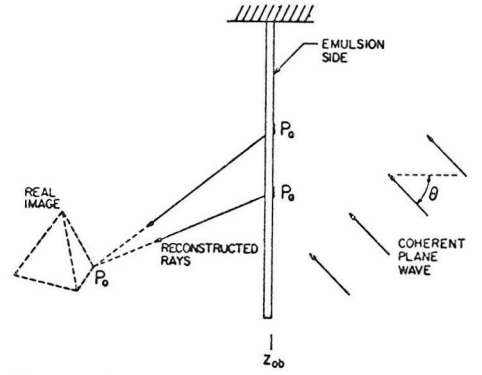

Fig. 3. Holographic wavefront reconstruction of pseudoscopic real image.

The holograms are made using the same lens and pinhole mounted on a 16 mm projector, whose optical system has been modified to permit illumination of the photographs with a He-Ne Laser. As shown in Fig. 2, a plane wave is beamed through an auxiliary lens, at z_c, onto the transparencies. The position of this lens, z_c, is adjusted to concentrate the light energy onto the pinhole. If the aperture is placed in the front focal plane of the camera lens, no auxiliary lens is required; if a larger or smaller separation is used, a concave or convex lens is required, respectively. Rather than move the projector, the high-resolution plane is mounted on the translator for this synthesis. Many possibilities exist for eliminating dead space between adjacent holograms, e.g., close spacing to provide extreme overlap; or precise fitting with a square aperture.

This method of holography is applicable to large objects which are naturally illuminated, and we have found the quality of plates made by this process to be very good due to the uniformity of exposure over the entire plate. Moreover, color holograms made with this method seem practical[7] using any standard color transparency film, e.g. Kodachrome Type II, in step 1 of the process and either a multiline laser such as the krypton-ion white light laser or a multicolor nonlaser spectral source for the illumination in step 2. In viewing, the same multicolor source may be used for illumination. In making a hologram of a transparency, as in step 2, it is not necessary to have as highly coherent a source as that required for an extended object; these considerations have recently been studied in detail[8,9]—the general requirement for small path length differences between the object and reference beams is easily satisfied in our case because of the small portions of the hologram individually exposed. An elegant way to minimize the path length differences when source coherency is limited is the imaged-grating technique of Upatnieks and Leith.[9] We have found an imaged zone plate to be compatible with step 2 of the color process described here, in which a plane wave reference is used; the requirement on source coherency is similarly reduced.

[1] R. V. Pole, *Appl. Phys. Letters* **10**, 20 (1967).

[2] A. W. Judge, *Stereoscopic Photography*, 3rd ed. (Chapman & Hall Ltd., London, 1950), p. 288.

[3] N. A. Valyus, *Stereoscopy* (Izdatel'stvo Akademii Nauk SSSR,

Moskva, 1962; English translation, Focal Press Ltd., London, 1966), pp. 88–94.
[4]G. Lippmann, *Compt. Rend.* **146,** 446 (1908).
[5]E. N. Leith and J. Upatnieks, *J. Opt. Soc. Am.* **53,** 1377 (1963).
[6]N. George and J. W. Matthews, *Appl. Phys. Letters* **9,** 212 (1966).
[7]Unpublished.
[8]A. W. Lohmann, *J. Opt. Soc. Am.* **55,** 1555 (1965).
[9]J. Upatnieks and E. N. Leith, presented at the April 1967, Columbus, Ohio meeting of the Optical Society of America, *J. Opt. Soc. Am.* **57** (1967).

APPENDIX III

THE EFFECTS OF EXTREME DISTORTION – A SIMPLE EXAMPLE

The effect of distortion in the Wild eyepiece may be characterized by a non-linear transformation of coordinates from object to image space. A good approximation for this transformation (cf. Fig. 12) is

$$\theta_i = \theta_o (1 - .34\ \theta_o^2) , \qquad \text{(III–1)}$$

$$\theta_i , \theta_o \lesssim \tfrac{1}{2} ,$$

where θ_o is the angle from the optical axis of the object point, and θ_i is the angle of the image point.

In general the effects of the individual aberrations cannot be separated. Therefore, although it is an inherent property of the holographic stereogram that lens distortion is unimportant by itself, we should also investigate its effect when combined with other forms of image degradation, particularly since distortion is independent of N.A. and is usually severe in eyepieces. A correct treatment of this problem would use the diffraction theory of aberrations. We shall treat a grossly simplified problem from a point of view based upon geometrical aberration theory, merely to illustrate the order of magnitude of the effect.

Consider an idealized one dimensional imaging system, where an object point at θ_o produces an image $g(\theta' - \theta'_i)$, symmetrical about θ'_i.

The unprimed coordinate refers to object space, the primed to image space, and the distortion is represented by

$$\theta'_i = \theta_o \left(1 - \frac{\theta_o^2}{3}\right) , \qquad \text{(III–2)}$$

$$\theta_i , \quad \theta_o \lesssim \tfrac{1}{2} .$$

Further, assume that a reverse imaging of a point at θ_i yields the image $h(\theta - \theta_o)$, symmetrical about θ_o, for any θ'_i, θ_o related by (III–2). (Note that the implied Green's function is not generally symmetrical to an interchange of $\theta \rightleftarrows \theta'$.) After a two step imaging process analogous to that of the holographic stereogram, an object point at θ_o is transformed into the function

$$f(\theta, \theta_o) = \int g(\theta' - \theta'_i)\, h(\theta - \phi_o)\, d\theta' , \qquad \text{(III–3)}$$

where ϕ_o is related to θ' by

$$\theta' = \phi_o \left(1 - \frac{\phi_o^2}{3}\right) , \qquad \text{(III–4)}$$

$$\theta' , \quad \phi_o \lesssim \tfrac{1}{2} .$$

If we expand $(\theta' - \theta'_i)$ in powers of $(\phi_o - \phi_o)$, and express $d\theta'$ as $\frac{d\theta'}{d\phi_o}\, d\phi_o$, we may rewrite (III–3) as

$$f(\theta, \theta_o) = \int g \left[(\phi_o - \theta_o) \left.\frac{d\theta}{d\phi_o}\right|_{\phi_o=\theta_o} + \frac{(\phi_o-\theta_o)^2}{2} \left.\frac{d^2\theta}{d\phi_o^2}\right|_{\phi_o=\theta_o} \right.$$

$$\left. + \frac{(\phi_o-\theta_o)^3}{6} \left.\frac{d^3\theta'}{d\phi_o^3}\right|_{\phi_o=\theta_o} \right] \cdot h(\theta - \phi_o) \cdot \frac{d\theta'}{d\phi_o} d\phi_o \quad . \qquad \text{(III–5)}$$

If we assume that the function g has approximate width $\Delta << 1$ (i.e. Δ is analogous to the angular resolution), and that $g' \sim O(g(0)/\Delta)$, then $g(\theta' - \theta'_i)$ and $d\theta'/d\phi_o$ can be expanded in powers of $(\phi_o - \theta_o)$. If we keep only the lowest order terms in $(\phi_o - \theta_o)$, (III–5) becomes

$$f(\theta, \theta_o) =$$

$$(1 - \theta_o^2) \int g[(\phi_o - \theta_o)(1 - \theta_o^2)] \, h(\theta - \phi_o) \, d\phi_o$$

$$-\theta_o (1-\theta_o^2) \int \{ (\phi_o-\theta_o)^2 \, g'[(\phi_o-\theta_o)(1-\theta_o^2)] \} \, h(\theta-\phi_o) \, d\phi_o$$

$$-2\theta_o \int \{(\phi_o-\theta_o) \, g[(\phi_o-\theta_o)(1-\theta_o^2)]\} \, h(\theta-\phi_o) \, d\phi_o \quad . \qquad \text{(III–6)}$$

The first integral is the convolution of an even function with another even function, and is therefore even in $(\theta - \theta_o)$ for a given θ_o. The second and third integrals however are convolutions of odd functions with an even

function, and hence are odd in $(\theta - \theta_o)$ for given θ_o – these two contributions result in an asymmetry of the response of the system, so that the center of gravity of $f(\theta, \theta_o)$ does not fall precisely on θ_o. These contributions are smaller than the first integral, however, by a factor of the order of Δ. The shift of the center of $f(\theta, \theta_o)$ from θ_o is therefore smaller than the width of f by a similarly small factor and is therefore negligible. Accordingly, we shall consider the effects of distortion to be negligible.

APPENDIX IV

ACHROMATIC INCOHERENT IMAGERY OF A FRESNEL ZONE PLATE WITH ONE OF THE FIRST ORDER DIFFRACTED WAVES ELIMINATED

The amplitude transmittance of a zone plate is given by

$$T_{a,b}(\bar{r}) = a + b\phi(\bar{r}) + b\phi^{*}(\bar{r}) \quad , \tag{IV-1}$$

where $a \geq 2b$ and ϕ is a phase factor associated with a spherical wavefront. The position on the zone plate is denoted by $\bar{r}$. Suppose we pass a monochromatic plane wave, or more generally a spherical wave through the plate, then through a uniform transparency and a lens which achromatically images the plate onto a conjugate plane. The wave due to a on the conjugate plane is

$$\text{wave}_{a} = \alpha a \phi'[\bar{r}(\bar{r}')] \quad , \tag{IV-2}$$

where α is a constant dependent upon the lens and transparency, and $\phi'[\bar{r}(\bar{r}')]$ is a phase factor dependent upon the conjugate plane coordinate $\bar{r}'$. The image point of $\bar{r}$ is given by the function $\bar{r}'(\bar{r})$ and $\bar{r}(\bar{r}')$ is the inverse of this. Similarly, the wave due to $b\phi(\bar{r})$ on the conjugate plane is

$$\text{wave}_{b\phi(\bar{r})} = \beta b \phi''[\bar{r}(\bar{r}')] \, . \tag{IV-3}$$

In practice $\alpha < \beta$, due to the transparency density. The wave due to $b\,\phi^*(\bar{r})$ is blocked, according to the discussion of Section 5.2. The intensity on the image plane is, in abbreviated notation,

$$I(\bar{r}') = \left| \alpha a \phi' + \beta b \phi'' \right|^2$$

$$= \alpha^2 a^2 + \beta^2 b^2 + \alpha a \beta b (\phi' \phi''^* + \phi'^* \phi''). \qquad \text{(IV–4)}$$

Due to the imaging arrangement, the optical path length from $\bar{r}$ to $\bar{r}'(\bar{r})$ is independent of the path, and therefore

$$\phi'[\bar{r}(\bar{r}')]\ \phi''^*[\bar{r}(\bar{r}')] = \phi^*[\bar{r}(\bar{r}')] \ . \qquad \text{(IV–5)}$$

Thus we may write

$$I(\bar{r}') = a' + b'\,\phi[\bar{r}(\bar{r}')] + b'\ \phi^*[\bar{r}(\bar{r}')] \ , \qquad \text{(IV–6)}$$

where

$$a' = \beta^2 b^2 \left\{1 + \left(\frac{\alpha a}{\beta b}\right)^2\right\} \ , \qquad \text{(IV–7)}$$

$$b' = \alpha a \beta b \ , \qquad \text{(IV–8)}$$

and

$$a' \geq 2b \ .$$

Comparison with (IV–1) yields

$$I(\bar{r}') = c\, T_{a'/c,\ b'/c}\,[\bar{r}(\bar{r}')] \quad . \tag{IV–9}$$

The intensity is proportional to the image of the amplitude transmittance of a zone plate equivalent to $T_{a,b}(\bar{r})$, i.e. having the same associated spherical wavefronts. The constant c may be chosen so that $a' + 2b' < c$, which is the condition for realizeability of the equivalent zone plate.

These results are independent of the exact form of the spherical wavefront. A spatially incoherent source, which may be viewed as a summation of incoherent monochromatic point radiators therefore yields essentially the same result. Furthermore, the results are independent of wavelength, and temporal incoherence is also unimportant.

APPENDIX V

SCALING AND RESOLUTION OF SCENIC HOLOGRAPHIC STEREOGRAMS

Reprint from: Society of Photo-Optical Instrumentation Engineers Seminar Proceedings 15, 161–165 (1968).

by

Nicholas George, J. T. McCrickerd, and M. M. T. Chang

California Institute of Technology

Pasadena, California

Abstract

Scaling of holographic stereograms in the ratio d/d' can be accomplished by using a spacing, d, between component photographs and a different spacing, d', between corresponding holograms. Scaling down of scenic holograms is desirable in order to increase visual impression of 3 dimensionality. Up-scaling of stereograms is called for to decrease the perspective of very small objects. Our analysis of resolution and depth of field shows the projector lens diameter to be the crucial factor in down-scaled stereograms, while the camera aperture is crucial in the up-scaled case. In d/d' scaling of a scene which extends from s_1 to ∞, the optimum projector aperture is given by $[2\lambda s_1/(d/d')]^{1/2}$; the component photographs should be taken with an aperture of $[2\lambda s_1]^{1/2}$, which may be altered by the root of the scale factor, by $[d/d']^{1/2}$ without seriously degrading the scaled-down stereogram's resolution. In the text numerical examples are given to illustrate the wide applicability of ordinary photographic apertures in making these down-scaled stereograms. Both linear and two-dimensional arrays of scaled-down scenic holograms have been made and these are described.

Introduction

An optical hologram of a scene has an ultimate resolution limit on the order of a wavelength. Often, as is the case for pictorial scenes, such a precise record is not particularly useful. In this paper we describe a generalized holographic-stereogram which is more practical in many cases than a hologram, and we discuss in some detail a useful scaling law relating the scene to image size as well as the choice of camera lens (f and D) and of related projector lens (f and D'). The depth of focus and the effect of scaling on an object at an arbitrary distance is treated in terms of basic photographic principles. We conclude with a description of some scenic stereograms which have been made of Yosemite Valley and also of the city of Pasadena using as a 2-dimensional platform the 9-story Millikan Library.

These stereograms are made by holographically recording an ensemble of ordinary photographic transparencies of the scene on a high resolution film plate. Our method is similar to that of R.V. Pole (Ref. 1); but as we have described earlier it differs in the respect that our photographs are taken sequentially (Ref. 2). This is of some advantage when the distance between component photographs need not be small, as with scenery; and of course it is essential to the scaling methods which we describe below. With this freedom of choice between aperture size, photograph size, and spacing, our stereograms are not resolution limited in the same physical manner as in integral photographs taken with the fly's-eye lens, although the general mathematical theory is applicable (Ref. 3).

Scaling of Holographic Stereograms

Photographs are taken of a scene from a regularly spaced array of points, such as the one-dimensional sequence shown in Fig. 1. Incoherent light received from the object points, P_1, P_2, P_3, is imaged on the film with the frames 1, ..., n recording the objects' parallax qualities. The camera, focal length f and diameter D, is focused at infinity; and, for simplicity, in the discussion of scenic photography, we assume that the object points are far enough removed from the camera to be sharply focused. Positives are made from the photographs, and these transparencies are projected as shown in Fig. 2 using a projector lens of focal length f and diameter D'. Frames 1 through n are projected sequentially using a monochromatic source (not shown) and recording holographically (at plane H in Fig. 2) as described in Ref. 2. A plane wave reference beam (not shown) is used.

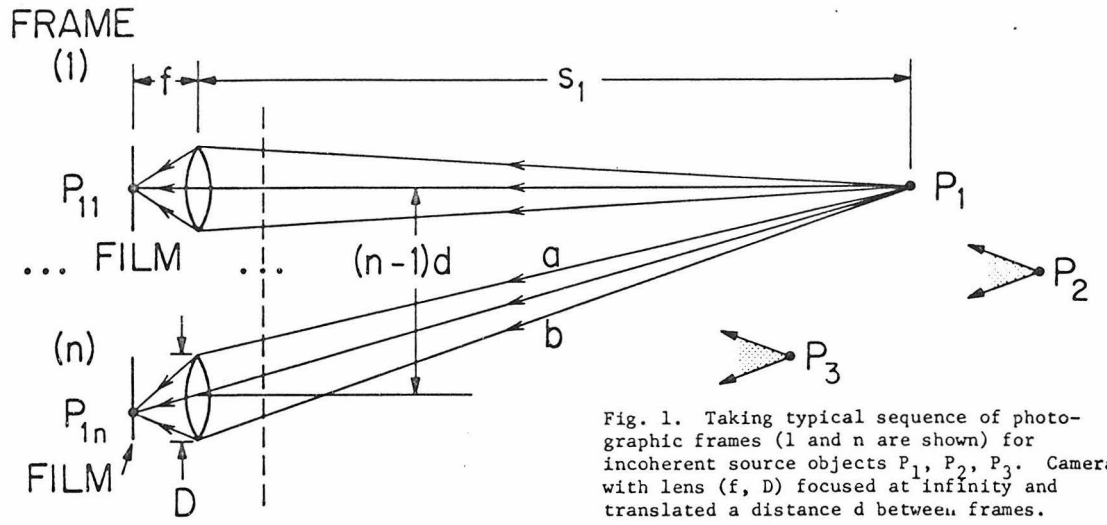

Fig. 1. Taking typical sequence of photographic frames (1 and n are shown) for incoherent source objects P_1, P_2, P_3. Camera with lens (f, D) focused at infinity and translated a distance d between frames.

For scenic stereograms, nd must be large enough to provide interesting perspective change; and yet, d should be small enough to approximate a continuous distribution of component photographs. In the taking sequence, the P_{1k} image of point P_1 occurs off of the frame center a distance $y_{1k} = (k - 1)fd/s_1$. In projection, the ray P'_{1k} intersects P'_{11} at a distance from the lens plane given by $s'_{1k} = f'd's_1/(fd)$ which we see is independent of the frame number k. Selecting the projection focal length $f' = f$, one sees that the scene is scaled in the ratio d'/d, i.e., $s'_1/s = d'/d$ or Fig. 1 is similar to Fig. 2. If enlargement of the component photographs is included, i.e., $m = y'_{1k}/y_{1k}$ and lens to film distances s_2, s'_2 instead of ∞ focus, then a more general scaling results, $s'_1/s = s'_2d'/(s_2dm)$ and we see that interesting angular distortions can be made by choosing s'_1/s_1 different from d'/d. An image is still formed.

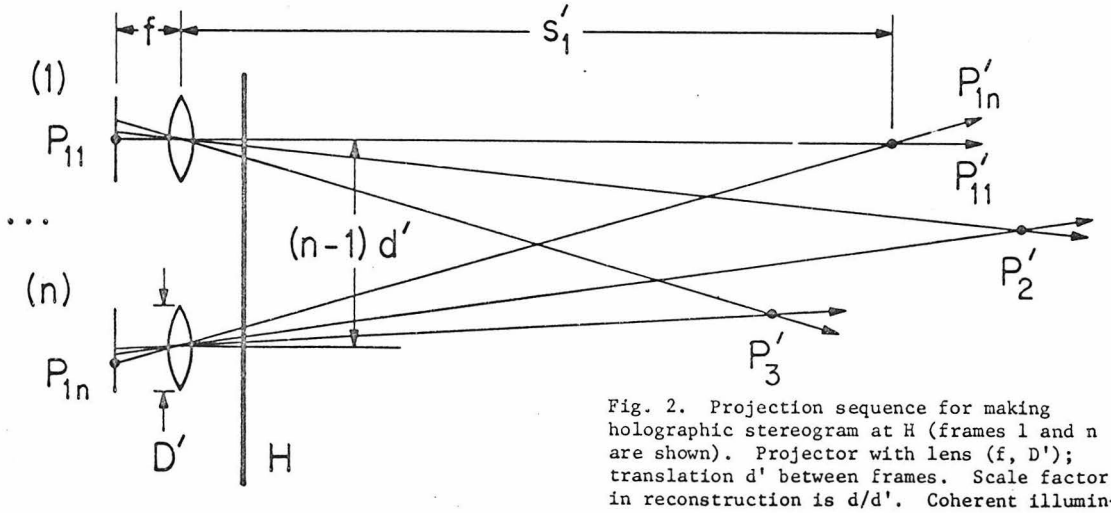

Fig. 2. Projection sequence for making holographic stereogram at H (frames 1 and n are shown). Projector with lens (f, D'); translation d' between frames. Scale factor in reconstruction is d/d'. Coherent illumination is used.

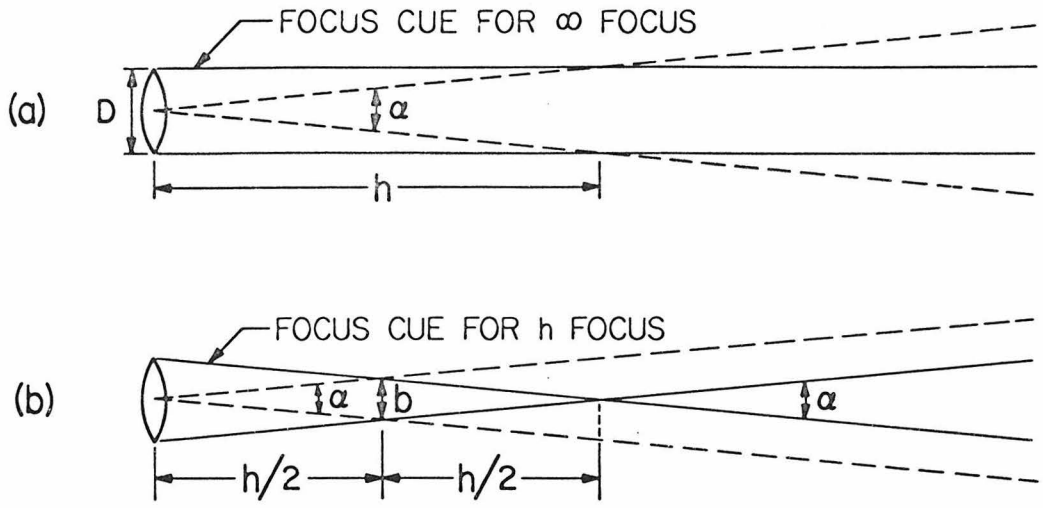

Fig. 3. (a) Determination of hyperfocal distance, h, based on desired angular resolution, α, and lens diameter D, using the focus cue for ∞ focus. (b) With lens focused at hyperfocal distance, depth of focus extends from half-hyperfocal distance to infinity. Degree of blurring, diameter b, at h/2 corresponds to same angular resolution α as at infinity.

Photographic Depth of Focus and Resolution Considerations

A very simple to use, yet rigorously correct, concept for depth of field calculations is that of the focus cue. This cue is defined as the cone which intersects the effective lens circumference and has its vertex in the object plane of focus. The degree of blurring in any plane closer or more distant than the focused plane is equal to the diameter of the focus cue in that plane. For example, a one inch lens set at f/4 has a focus cue of diameter 1/4" at the lens. If the lens is focused at 10 feet, the cue has zero blurring there, but has 1/8" diameter blur at either five feet or fifteen feet. Alternatively, if the lens is set to f/2 and focused at infinity, a blurring of 1/2" will occur regardless of the object distance, since the focus cue in this case is a cylinder of 1/2" diameter extending to infinity.

For photographic purposes, one is frequently interested in angular, rather than absolute resolution. If, for example, we specify an angular resolution of 1/1000 radian, then the one inch f/2 lens focused at infinity will provide sufficient angular resolution beyond 500 inches, and we refer to this as the hyperfocal distance, h, see Fig. 3a. However, by focusing at h, the lens has sufficient angular resolution from h/2 to infinity, as shown in Fig. 3b.

While the angular resolution determines the apparent sharpness of a photograph, the absolute resolution is often easier to specify in a particular imaging problem. For example, if we wish our camera to resolve a person's eyes at 100 feet, we simply specify that the focus cue have a diameter of $\lesssim 1$ inch at this distance. For a specified absolute resolution, it is also easy to use the focus cue concept to show that the lens should optimally be focused at the middle plane of the object's total depth.

At a given aperture, the lens resolution also restricts the photograph's angular resolution. This, and the film's resolution, impose limits on the amount of sharpening possible by stopping down of the lens aperture. For example, if film limitations are negligible and the lens is diffraction limited, the absolute diffraction blurring is $\sim\lambda/\alpha$, where λ is the wavelength of light, and α is the angle of divergence of the focus cue. Focusing at the center of the object of depth L, the maximum depth-of-focus blurring is $\sim\alpha L/2$. An optimum focus cue, therefore, has a divergence $\alpha = [2\lambda/L]^{1/2}$, and if s is the camera-object distance, the optimum aperture is $\sim s(2\lambda/L)^{1/2}$, corresponding to an angular resolution of $(1/s)(\lambda L/2)^{1/2}$ radians. Similarly, if one wishes to optimize angular resolution, it can be shown that the camera should be focused at $s = 2s_1s_2/(s_1 + s_2)$ using an aperture of $[\lambda s(s_1 + s_2)/(s_2 - s_1)]^{1/2}$ to attain an angular resolution of $[\lambda(s_2 - s_1)/(2s_1s_2)]^{1/2}$

where s_1 is the minimum object distance, and s_2 the maximum. In either case, the optimum aperture size increases as the half power of the scale of the recorded scene, and the angular blurring of the optimized system decreases by the same quantity.

Stereogram Resolution and (Distortionless) Scaling

The holographic stereogram process involves two stages of imaging to which the above considerations apply. The only difference is that the blurring is multiplied by a factor such as $\sqrt{2}$ to account for the two stages.

Scaling of the stereogram requires additional considerations, however. Since the angular blurring decreases like the half power of the scaling of the scene, the resolution of an optimized scaled stereogram is determined primarily by the lens arrangement used for the smaller scale. Therefore, the lens size used in the larger scale may vary, up or down, by a factor of the half power of the scale ratio without seriously affecting resolution. Therefore, the lens size for the larger scale may be the same as for the small scale, as is also obtained from more restrictive considerations based solely on diffraction; or it may increase by as much as the scale factor, which is the anticipated result if diffraction is ignored and all of the focus cues are scaled along with the scene. And although the film may sometimes limit the attainable resolution in photographing a scene, this limitation is usually no more stringent than the resolution limitations of the small scale projection step and can often be disregarded.

This analysis has been based on a compromise between depth of focus blurring and diffraction blurring. It should be noted, however, that it is possible to eliminate depth of focus blurring for particular planes of interest by techniques similar to those recently described in the literature. (Ref. 4, 5). If this approach to stereogram viewing is taken, it will be advantageous to optimize the information content by using even larger apertures throughout.

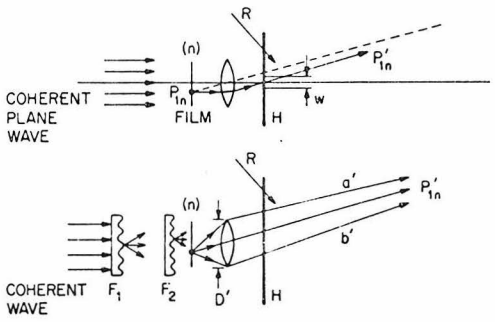

Fig. 4. Detail of hologram (H) for n^{th} frame: transform width (w) if coherent plane wave illumination (upper) or wider pencil of rays a', b' if frosted glass diffusers F_1, F_2 are used (lower). Projected rays from only one image point P_{1n} are shown.

Experiments

Several scenic holograms have been made in order to study scaling effects. The component photographs have been taken with a 16mm. motion picture camera and also with a 35mm. single lens reflex camera. A single frame of the projection sequence is illustrated in Fig. 4. If the film record has fine detail of ν lines/mm. recorded near P_{1n}, then the transform width w for the coherent plane wave illumination is approximately given by $w = 2\lambda f\nu$. With picture detail ν = 20 lines/mm. and f = 50 mm., this width is only about 1 mm. However, in the projection the rays holographically recorded can certainly extend as far as D' = d'D/d in the transform plane; this is the previously described limit obtained by directly scaling the focus cues, a - b in Fig. 1 in proportion to a' - b' in Fig. 2 as d/d'.

In our experiments, typically, this optimum value of D' greatly exceeded the transform width. In principle, this optimum width can be obtained by filling in or nesting a cluster of repeated exposures of the same hologram of width w within the diameter D'. In practice this incoherent-transform-hologram is easily obtained experimentally using a ground glass diffuser in back of the film transparency. The most uniform distribution of light in the transform plane resulted from the cascade shown: F_1 is a piece of non-glare glass intended for framing portraiture; and F_2 is frosted glass. The non-glare glass is too regular to be used alone, but in cascade it can be positioned to adjust the angular spectrum and the level of the illumination. It should be emphasized that the hologram plate need not be located physically in the transform plane of the lens. This is important, practically, since the front focal plane of many excellent photographic lenses is located less than 1 cm. from the first lens element and introduction of the planar reference beam R would be

awkward.

A two-dimensional stereogram is shown in Fig. 5. together with two one-dimensional arrays printed to different scales, d/d'. The first array serves to illustrate the lattice relationship of the component photographs (elimination of the diffuser enhances the deleterious edge or screen effect and is done here for clarity of presentation only). The two linear arrays show the effect of varying amounts of overlap using the same component photographs, see Fig. 6. Important detail in this scene occurs beyond 300 feet, thus with a 20:1 scale the corresponding detail in the reconstruction is beyond 15 feet. Excellent stereo effects are observed using a 6 foot base line with d in the range from one to four inches. A one-inch spacing provides a sampling interval of one minute of arc at 300 feet which is virtually continuous for visual observation (Ref. 6).

An extremely wide angle lens is a good choice for taking the component photographs, since distortions cancel in the projection sequence if the same lens is used, see Figs. 1 and 2. Panoramic effect can also be achieved with a normal photographic lens by taking several component photographs with overlapping fields of view at each point of the array. These are easily superimposed holographically in the projection sequence. It is important to preflash the hologram plate in order to obtain equal brightness in reconstructions from overlapping or superimposed holograms made with a fixed exposure (Ref. 7).

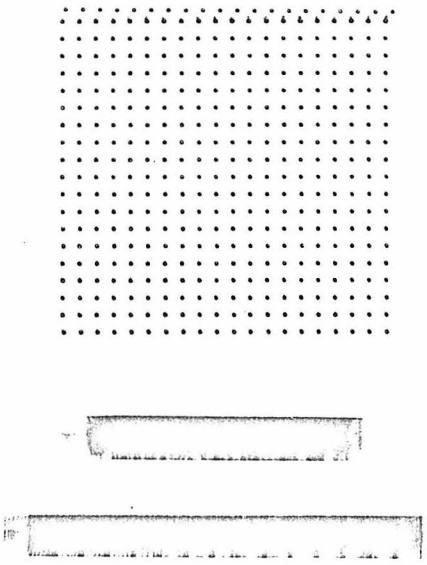

Fig. 5. Holographic Stereograms: Two-dimensional array (upper) without diffuser, twenty frame overlapping stereogram of Yosemite Valley scale ratios 20:1 (middle) and 13.3 : 1 (lower).

Fig. 6. Half Dome, Yosemite National Park; component photograph for the stereogram of Fig. 5.

Conclusions

The proposed method for scaling holographic stereograms has been applied with considerable success to down-scaling of an object of large dimensions. The use of sequential component photographs is essential to this scaling, as well as being a rather practical way of attaining high picture quality. Stereoscopic reconstructions exhibiting sharp focus and negligible screen effect have been made using multiply overlapping component holograms made with a diffuser and a relatively large diameter lens in the projection step.

The authors would like to acknowledge helpful discussions with J.W. Matthews. The research was supported in part by the Electronics Division of the Air Force Office of Scientific Research.

References

1. R.V. Pole, Appl. Phys. Letters 10, 20(1967).
2. J. T. McCrickerd and Nicholas George, Appl. Phys. Letters 12, 10(1968).
3. C. B. Burckhardt, J. Opt. Soc. Am. 58, 71(1968).
4. G. W. Stroke and R. G. Zech, Physics Letters 25A, 89(1967).
5. G. W. Stroke, G. Indebetouw, and C. Puech, Physics Letters 26A, 443(1968).
6. M. Born and E. Wolf, "Principles of Optics" (Pergamon Press, Inc., New York, Third (Revised) Edition 1965), pp. 415-416.
7. J. C. Wyant and M. Parker Givens, J. Opt. Soc. Am. 58, 357(1968).

REFERENCES

1. T. Kallard (ed.), Holography, State of the Art Review – 1969, Optosonic Press (1969).

2. R. P. Chambers and J. S. Courtney-Pratt, "Bibliography on Holograms," Journal of the S.M.P.T.E. 75, 373-435 (1966).

3. R. P. Chambers and J. S. Courtney-Pratt, "Bibliography on Holograms-II," Journal of the S.M.P.T.E. 75, 759-809 (1966).

4. R. P. Chambers and B. A. Stevens, "Bibliography on Holograms-III," Journal of the S.M.P.T.E. 76, 392-395 (1967).

5. J. W. Matthews, Scientific Report No. 7 under U.S. Air Force Contract AF49(638)-1322, 1967 (unpublished); Ph.D. thesis, California Institute of Technology, 1967 (unpublished).

6. M. Born and E. Wolf, Principles of Optics (second edition), The MacMillan Co., 143-147 (1964).

7. P. P. Sokolov, Auto Stereoscopy and Integral Photography by Professor Lippmann's Method, Moscow State University Press (1911). (The existence of this book has not been confirmed; the only known reference to it appeared in: N.A. Valyus, Stereoscopy, Focal Press, 417 (1966).)

8. M. Born and E. Wolf, op. cit., 435-445.

9. G. Lippmann, "Epreuves Reversibles. Photographies Integrales," Compt. Rend. 146, 446-451 (1908).

10. C. B. Burckhardt, "Optimum Parameters and Resolution Limitation of Integral Photography," J. Opt. Soc. Am. 58, 71-76 (1968).

11. W. J. Smith, Modern Optical Engineering, McGraw-Hill, 305-307, 398-405 (1966).

12. R. V. Pole, "3–D Imagery and Holograms of Objects Illuminated in White Light," Appl. Phys. Letters 10, 20-22 (1967).

13. E. N. Leith and J. Upatnieks, "Wavefront Reconstruction with Continuous-Tone Objects," J. Opt. Soc. Am. 53, 1377-1381 (1963).

14. N. George and J. W. Matthews, "Holographic Diffraction Gratings," Appl. Phys. Letters 9, 212-215 (1966).

15. M. Born and E. Wolf, op. cit., 206-207.

16. Ibid., 213.

17. Ibid., 437.

18. Ibid., 399.

19. A. W. Lohmann, "Grating Diffraction Spectra as Coherent Light Sources for Two or Three Beam Interferometry," Optica Acta 9, 1-12 (1962).

20. A. W. Lohmann "Wavefront Reconstruction for Incoherent Objects," J. Opt. Soc. Am. 55, 1555-1556 (1965).

21. R. E. Brooks, L. O. Heflinger, and R. F. Wuerker, "Pulsed Laser Holograms," I.E.E.E.-QE-2, 275-279 (1966).

22. E. N. Leith and J. Upatnieks, "Holography with Achromatic Fringe Systems," J. Opt. Soc. Am. 57, 975-980 (1967).

23. M. Kato and T. Suzuki, "Fourier-Transform Holograms by Fresnel Zone-Plate Achromatic-Fringe Interferometer," J. Opt. Soc. Am. 59, 303-307 (1969).

24. J. T. McCrickerd and N. George, "Holographic Stereogram from Sequential Component Photographs," Appl. Phys. Letters 12, 10-12 (1968).

25. P. J. Van Heerden, "Theory of Optical Information Storage in Solids," Applied Optics 2, 393-400 (1963).

26. A. Van der Lugt, "Signal Detection by Complex Spatial Filtering," I.E.E.E.-IT-10, 139-145 (1964).

27. G. W. Stroke and R. G. Zech, "A Posteriori Image-Correcting 'Deconvolution' by Holographic Fourier-Transform Division," Physics Letters 25A, 89-90 (1967).

28. A. W. Lohmann, "Matched Filtering with Self Luminous Objects," Applied Optics 7, 561-563 (1968).

29. M. Born and E. Wolf, op. cit., 213.

30. Ibid., 225.